



## Spatial Distribution of Ammonia Emissions on the Territory of the Czech Republic

M. Zapletal and P. Chroust

Centre for Environment and Land Assessment - Ekotoxa Opava, Horní nám. 2, 746 01 Opava, Czech Republic

### Abstract

Modeling of the spatial distribution of ammonia ( $\text{NH}_3$ ) emissions on the territory of the Czech Republic within a 5x5 km grid is essential condition for the modelling of atmospheric transport and deposition flux of reduced nitrogen compounds and exceedances of critical loads of nutrient nitrogen. Spatial distribution of ammonia emissions is a suitable tool for strategy identification of ammonia emission reduction. Key input data to the model of distribution of ammonia emission are detailed data on number and positioning of cattle, horses, sheep, goats, pigs and poultry, data on mineral fertilisers usage, data on the industrial sources and processes, data on the other anthropogenic sources and land use data. For an assessment of total ammonia emission originating from livestock breeding the emission factors have been applied. Total ammonia emissions in 2002 were calculated as a sum of ammonia emission from livestock breeding, emission from mineral fertilisers usage, emission from industrial sources and processes and emission produced by human population on the territory of the Czech Republic on a 5x5 km grid. Total ammonia emission in the Czech Republic in 2002 was estimated to be 72.3 kt  $\text{NH}_3$  year<sup>-1</sup>. Ammonia emission from agricultural sources was estimated to be 68.4 kt  $\text{NH}_3$  year<sup>-1</sup>. There from cattle 29 kt  $\text{NH}_3$  year<sup>-1</sup>, pigs 29.9 kt  $\text{NH}_3$  year<sup>-1</sup>, poultry 7.5 kt  $\text{NH}_3$  year<sup>-1</sup>, horses, sheep and goats 0.21 kt  $\text{NH}_3$  year<sup>-1</sup>, mineral fertilisers usage 1.7 kt  $\text{NH}_3$  year<sup>-1</sup>. Ammonia emission from industrial sources and processes was estimated to be 0.8 kt  $\text{NH}_3$  year<sup>-1</sup>. Ammonia emission from human population was estimated to be 3.1 kt  $\text{NH}_3$  year<sup>-1</sup>.

### Introduction

Atmospheric pollution by ammonia emissions involves an important environmental problem. Because of wet and dry ammonia depositions contribution to acidification and eutrofisation of ecosystems, ammonia is regarded to be a significant agent participating on present gradual extinction and damage of forests. The source of ammonia emissions in the Czech Republic are namely agricultural activities (housing of cattle, manure storage and application, fertilisers application) (Zapletal, 1997, 1998, 2001, 2002). Industrial production (heat treatment of coal, chemical industry) and other sources (transport, emissions from human population) represent a less contribution to ammonia emissions. The main source of ammonia in the nature is its generation due to linkage of atmospheric nitrogen through the bacterial processes cycling in a soil and consequent release to the atmosphere. The model on spatial distribution of emissions and deposition flux concentrations of ammonia on the territory of the Czech Republic on a 10x10 km grid in 1994 is presented in the work Zapletal (1997).

This study includes description, application and the results of modelling the spatial distribution of ammonia emissions on the territory of the Czech Republic on a 5x5 km grid level using emission model and detail emission inventory of all significant ammonia emission sources. Exact ammonia emissions spatial distribution is the essential input into transport and deposition models for a purpose of modelling atmospheric transport and deposition flux of reduced nitrogen compounds and for evaluation exceedances of critical loads of nitrogen and acidity on the territory of the Czech Republic. Spatially distinguished ammonia emissions are a useful aid for the determination strategy and tools of abatement of ammonia emissions.

### Methods

#### Source Data

Ammonia emissions from livestock breeding (emissions from housing, manure and sewage storage, fertilisers and sewage application on field, emissions from grazing period), emissions from application

mineral fertilisers used in agriculture, technologic emissions from industrial sources and emissions from people population were included in calculation of the total ammonia emission on the territory of the Czech Republic.

The main source of data for determination of spatial distribution of ammonia emissions on the territory of the Czech Republic was the Register of stables in 2001 and 2002 (Zapletal et al., 2004), including detail data on breeding and location of livestock stables (firstly cattle), and the Soil Register incorporating information on land use (Zapletal et al., 2004). Data on pigs and poultry numbers were derived from the database of the State Veterinary Administration in Liberec (Zapletal et al., 2004). The details for assignment of spatial distribution of ammonia emissions originating from industrial sources were provided by the Czech Hydrometeorological Institute (CHMI, 2002). Information about population of the Czech Republic were derived from available data of the Czech Statistical Office (CSO, 2003).

### Methodology of Modeling the Spatial Distribution of Ammonia Emission

The ammonia emissions from livestock breeding were calculated using livestock numbers and average annual emission factor. The emissions from breeding cattle, horses, sheep and goats were calculated separately for all individual stables. Emissions from pig-breeding and poultry-farming were calculated for all sources recorded in the respective cadastral region. Spatially differentiated data on numbers of water poultry were not available. Emissions calculated in different spatial detail were summarised in GIS to a 5x5 km grid covering entire territory of the Czech Republic.

Emission factors have been used to assess the total ammonia emission from livestock breeding including four types of production NH<sub>3</sub> emissions (emissions from housing, emissions from farm-manure storage, emissions from farm-manure application and emissions from grazing period). These factors were suggested for individual livestock classes according to actual legislation (MECR, 2002) and conclusions of the Ammonia Expert Panel of the UN ECE (Hoek, 1998). Average emission factors used for cattle, pigs, poultry, horses, sheep and goats are presented in Table 1.

Emission factors have been used for the following animal categories: dairy-cows, calves, bulls, heifers, sucking-pigs, sows, fattening pigs, layers, broilers, geese and ducks. Emission factor for sows was determined as a weighted average of factors of sows and in-pig sows. Emission factors for turkey hens, turkey cocks, goats, sheep and horses were applied according to results of the Ammonia Expert Panel of the UN ECE (Hoek, 1998).

Emissions from application of mineral fertilisers have been calculated according to area of agricultural land in individual land parcels (Zapletal et al., 2004) in a 5x5 km grid including arable land, gardens, vineyards and hop-gardens, excluding pastures and meadows that are not supposed to be fertilised with mineral fertilisers, according to average of converted nitrogenous fertilisers consumption on 1 ha of agricultural land (on basis of the Czech Statistic Office data) (CSO, 2003) and according to average factor of nitrogen loss from applied nitrogenous mineral fertilisers (2.94 %) (Dragosits et al., 1998). For an assessment of ammonia emissions from industrial sources, the Register of Emissions and Air Pollution Sources (CHMI, 2002) was used. Ammonia emissions from human population have been derived from database of the Czech Statistical Office (CSO, 2003) and from average amount of ammonia emitted by an individual, i.e. 0.3 kg NH<sub>3</sub> man<sup>-1</sup> year<sup>-1</sup> (Klaassen, 1990).

The spatial scale of ammonia emissions varies with source data. Summarisation of source data of different spatial detail (cadastral area, parishes, point sources, land parcels) was carried out by means of the tools for spatial analyse in GIS.

## Results and Discussion

The distribution of ammonia emissions is extremely variable in regional scale (district, county) and in local scale (surrounding of emission sources and stables). Ammonia emissions are concentrated in intensively covered agrarian areas at close vicinity of stables and storage facilities and industrial sources. Dominant share on the total ammonia emission presents emission from agricultural production (ranging as far as 95% of total emission), first of all emission from livestock breeding (housing, storage and application of manure, waste and grazing). In 2002, emissions from technologic sources participated on total ammonia emissions in the Czech Republic by 1 % and emissions from human population by 4 %.

## Agricultural Sources

Emission factors, animal numbers and ammonia emissions for individual categories of animals in the Czech Republic in 2002 are presented in Table 1.

**Table 1. Emission factors (kg NH<sub>3</sub> animal<sup>-1</sup> year<sup>-1</sup>), numbers of animals and ammonia emissions (kt NH<sub>3</sub> year<sup>-1</sup>) for individual categories of animals in the Czech Republic in 2002**

Animal category	Emission factor (kg NH <sub>3</sub> animal <sup>-1</sup> year <sup>-1</sup> )	Animal numbers	Emission (kt NH <sub>3</sub> year <sup>-1</sup> )
Dairy cows	27.9	502 500	14.0
Cows	16.2	131 300	2.1
Heifers	16.2	341 500	5.5
Calves	16.2	226 400	3.7
Bulls	16.2	221 300	3.6
Other cattle	16.2	4 500	0.1
Total cattle		1 427 500	29.0
Total sows	17.44	289 000	5.0
Sucking-pigs	6.5	735 200	4.8
Pigs	8.3	2 423 200	20.1
Total pigs		3 447 400	29.9
Broilers	0.21	21 950 100	4.6
Layers	0.27	6 704 700	1.8
Turkey cocks and hens	0.92	893 600	0.8
Other poultry	0.21	288 100	0.1
Total scraping poultry		29 836 500	7.2
Geese and ducks	0.73	306 500	0.2
Total poultry		30 143 000	7.5
Horses	8	14 000	0.11
Sheep	1.34	65 000	0.09
Goats	1.34	3 800	0.01

Ammonia emissions from predominant sources, i.e. emissions from livestock breeding, tend to occur on specific land use types. Emissions from housing of livestock and from storage of farm manures are defined spatially by a zone of agricultural source. Emissions from applied farm manures and mineral fertilisers occur in a point of application, i.e. on fields (arable land). Ammonia emissions emitted during grazing period of cattle, horses, sheep and goats are linked spatially with pastures.

Predominant part on the total ammonia emissions from livestock breeding pertains to pig breeding (45 %) and cattle breeding (44 %), i.e. together nearly 89 %. A part of poultry farming emissions is about 11 %. A part of emissions from breeding other livestock categories (horses, sheep, goats) is rather marginal (less than 1 %). Small equipments of capacity to 179 cattle pieces share on ammonia emissions from cattle breeding mostly (more than 58 % of total emissions from cattle breeding in the Czech Republic).

## Mineral Fertilisers

Ammonia emissions from application mineral fertilisers on the territory of the Czech Republic in 2002 have been estimated to be in total 1.7 kt NH<sub>3</sub> year<sup>-1</sup>. The total consumption of nitrogenous mineral fertilisers in the time period 1994/1995 to 1998/1999 decreased approximately by 10 % and raised during the period 1998/1999 to 2000/2001 again by about 13 %.

## Industrial Sources and Human Population

From the Register of Emissions and Air Pollution Sources have been selected 252 industrial (technologic) ammonia emissions sources. These sources were localised on the territory of the Czech Republic by means of geographic coordinates and according to cadastral parcels classification. The total ammonia emission from industrial sources recorded in the Czech Republic in 2001 amounts 0.8 kt NH<sub>3</sub> year<sup>-1</sup>.

Ammonia emission from human population on the territory of the Czech Republic calculated on basis of the data provided by the Census 2001 (CSO, 2003), was estimated to be 3.1 kt NH<sub>3</sub> year<sup>-1</sup>.

### Total Ammonia Emission

Total ammonia emission for the Czech Republic in 2002 calculated as a sum of ammonia emissions from cattle breeding, from mineral fertilisers application, from emissions produced by industry and human population was estimated to be 72.3 kt NH<sub>3</sub> year<sup>-1</sup>. The spatial distribution of the total ammonia emissions (kg NH<sub>3</sub> – N ha<sup>-1</sup> year<sup>-1</sup>) from agricultural and other sources in the Czech Republic on a 5x5 km grid resolution in 2002 is represented in Figure 1.

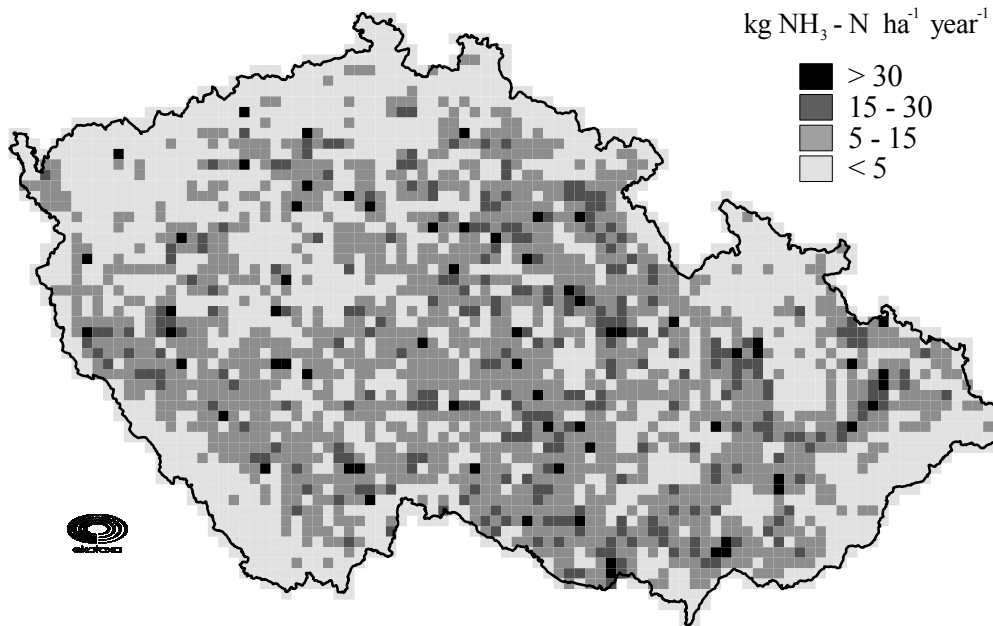


**Figure 1. Ammonia emissions (kg NH<sub>3</sub> – N ha<sup>-1</sup> year<sup>-1</sup>) from agricultural and other sources in the Czech Republic on a 5x5 km grid in 2002**

### Conclusions

The actualised data on ammonia emissions including their location have been used for modelling the spatial distribution of ammonia emissions on the territory of the Czech Republic in 2002. The total values of ammonia emissions have been computed as a sum of ammonia emissions from livestock breeding, emissions from mineral fertilisers application, emissions from industrial sources and emissions produced by human population. These were distributed by means of GIS tools into a regular 5x5 km grid covering all of the territory of the Czech Republic.

From the results of spatial emission balance it follows that national emission ceiling for the Czech Republic by 2010 (80 kt NH<sub>3</sub> year<sup>-1</sup>) (MECR, 2003) was not exceeded by the actual ammonia emission level in 2002 (72.3 kt NH<sub>3</sub> year<sup>-1</sup>). A great scope at achievement emission ceiling by 2010 can be found at abundance good agricultural practice and spatial usage of verified technologies decreasing ammonia emissions from agricultural production.

### Acknowledgement

This study was funded by the Ministry of Environment of the Czech Republic (project VaV/740/1/02).

## References

- CHMI. 2002. Air pollution in the Czech Republic in 2001. The Czech Hydrometeorological Institute, Prague, 161 pp.
- CSO. 2003. Statistical Yearbook of the Czech Republic 2002. The Czech Statistical Office, Prague, 360 pp.
- Dragosits, U., M.A. Sutton, C.J. Place, and A.A. Bayley. 1998. Modelling the spatial distribution of agricultural ammonia emissions in the UK. In: van der Hoek, K.W, J. W. Erisman, S. Smeulders, J.R. Wisniewski, and J. Wisniewski (eds.), *Nitrogen, the Confer-N-s: Proceedings of First International Nitrogen Conference*, March 23-27, 1998. Noordwijkerhout. The Netherlands, Elsevier Science, Amsterdam, pp. 195 – 203.
- Hoek van Der, K.W. 1998. Estimating Ammonia Emission Factors in Europe: Summary of the Work of the UNECE Ammonia Expert Panel. *Atmospheric Environment* 32: 315-316.
- Klaassen, G. 1990. Emissions of ammonia in Europe. IIASA WP-90-68. Laxenburg, Austria, 39 pp.
- MECR. 2002. Decree of the Government of the Czech Republic No. 353/2002. Ministry of the Environment of the Czech Republic, Prague, 55 pp. (in Czech)
- MECR. 2003. Decree of the Government of the Czech Republic No. 417/2003. Ministry of the Environment of the Czech Republic, Prague, 2 pp. (in Czech)
- Zapletal, M. 1997. Atmospheric deposition of acidifying components on the territory of the Czech Republic. (Ph.D. Thesis., The Technical University of Mining and Metallurgy at Ostrava). Silesian University at Opava, Opava, 161 pp. (in Czech, summary in English)
- Zapletal, M. 1998. Atmospheric deposition of nitrogen compounds in the Czech Republic. *Environmental Pollution* 29: 305-311.
- Zapletal, M. 2001. Atmospheric deposition of nitrogen and sulphur compounds in the Czech Republic. *The ScientificWorld* 1 (S2): 294-303.
- Zapletal, M. 2002. Atmospheric deposition of nitrogen and sulphur compounds in the Czech Republic. In: Galloway, J., E. Cowling, J.W.Erisman, J. Wisniewski, and C. Jordan (eds.): *Optimizing Nitrogen Management in Food and Energy Production and Environmental Protection*. Contributed Papers from the 2<sup>nd</sup> International Nitrogen Conference, 14 –18 October 2001. Potomac, Maryland, USA, Lisie, Abingdon, Exton, Tokyo, pp. 294-303.
- Zapletal, M., P. Chroust, D. Kuňák, M. Sáňka, M. Fara, I. Skořepová, D. Fottová, T. Pačes, H. Kazmarová, P. Čupr, E. Budská, P. Fabiánek, and J. Seják. 2004. Efficiency investigation of measures for reduction of air pollution based on abatement of negative effects of pollutants on environmental compartments and human health. Project VaV 740/1/02. Ekotoxa Opava, Opava, 600 pp. (in Czech, summary in English)



## Characterization of Particulate Emission from Animal Feeding Operations with Three-wavelength Lidar Using Simultaneous In-situ Point Measurements as Calibration Reference Sources

Vladimir V. Zavyalov<sup>1</sup>, Gail E. Bingham<sup>1</sup>, Thomas D. Wilkerson<sup>1</sup>, Jason Swasey<sup>1</sup>, Christian Marchant<sup>1</sup>, Christopher Rogers<sup>1</sup>, Randy Martin<sup>2</sup>, Phil Silva<sup>2</sup>, and Vishal Doshi<sup>2</sup>

<sup>1</sup>Space Dynamics Laboratory, 1695 North Research Parkway, North Logan, UT 84341  
Tel: 435-797-4116 Fax: 435-797-4599 vladimir.zavyalov@sdl.usu.edu

<sup>2</sup>Utah State University, Logan, UT 84322

### Abstract

Lidar (Light Detection And Ranging) provides the means to quantitatively evaluate the spatial and temporal variability of particulate emissions from agricultural activities, including animal feeding operations. A three-wavelength portable scanning Lidar system built at the Space Dynamic Laboratory (SDL) is used to extract optical properties of the particulate matter from the return Lidar signal and to convert these optical properties to physical parameters including the spatial distribution of particulate concentration around the agricultural facility and its temporal variations. The inversion algorithm developed to retrieve physical parameters of the particulate matter takes advantage of measurements taken simultaneously at three different wavelengths (355, 532, and 1064 nm) and allows us to estimate the particle size distribution in the emitted plume as well; however, quantitative evaluation of particulate optical and physical properties from the Lidar signal is complicated by the complexity of particles composition, particle size distribution, and environmental conditions such as the ambient humidity. Additional independent measurements of particulate physical and chemical properties are needed to unambiguously calibrate and validate the particulate physical properties retrieved from the Lidar measurements. In this paper we present results of the particulate emission characterization obtained by simultaneous remote measurements with Lidar and point measurements at the feeding operation site with standard equipment including optical particle counters, portable PM<sub>10</sub> and PM<sub>2.5</sub> ambient air samplers, multistage impactors, an aerosol mass spectrometer, and ion chromatography.

### 1. Introduction

Agricultural operations produce a variety of particulates and gases that influence ambient air quality and are important to the well-being of humans, animals, and plants. Concentrated Animal Feeding Operations (CAFO) are being investigated by government regulators as one of the major sources of air and water pollutants. The United States Department of Agriculture (USDA) and Agriculture Research Service (ARS) have developed a program to measure the level of pollutants crossing the CAFO boundary and the source and transport phenomenon associated with the pollutant release. The federal government regulations of CAFO are based on point-source pollution measurements located around CAFO facilities. These localized point measurements cannot adequately determine the spatial and temporal distribution of pollutant emission over extended atmospheric regions. Additionally, variations in environmental conditions and pollutant transport activities make it practically and economically infeasible to monitor actual pollutant source strength using point sensors. Lidar (Light Detection And Ranging) technology (Measures, 1984) provides a means to derive quantitative information of particulate spatial distribution and optical properties over remote distances using one instrument located at a single convenient point. The Space Dynamics Laboratory (SDL) at Utah State University has teamed with ARS researchers to build a Lidar system for remote sensing of pollution from agricultural activities including CAFO. A combination of scanning geometry with a high repetition rate laser allow us to measure representative three dimensional (3D) cross sections of particulate clouds in a reasonable time of a few minutes. For agricultural assessment, the most representative Lidar scan pattern employs repeated vertical scans of the atmosphere on the upwind and downwind sides of a pollutant emission source. When combined with wind speed information, this pattern allows the estimate of source flux rates using the input-minus-output flux difference method (Hipps, 1995). High spatial resolution of 5m and 3D representation of the measured distribution makes the Lidar system a unique instrument for particulate flux measurements and monitoring of flux temporal and spatial variations.

The Lidar technique measures the return signal of laser light scattered by the atmosphere and is equivalent to the integral of the backscatter cross section of the particles (aerosols) present in the atmosphere with the particle size distribution as the weighting function. The aerosol backscatter cross section is uniquely determined by the physical and chemical properties of the aerosols (size, shape, and complex refractive index) and the laser wavelength. The wavelength dependence on the backscatter coefficient is mainly determined by the aerosol size distribution and refractive index. Different aerosol types have different refractive indices and size distributions, which implies that it is possible to discriminate aerosol types according to the wavelength dependence measured by a multiple wavelength Lidar. Using backscatter coefficients measured at several laser wavelengths, the physical properties of aerosols, including size distribution and particle concentration, can be retrieved by determining a solution to the Mie integral equations describing scattering properties of the aerosol (Bockmann, 2001). Thus a multiwavelength Lidar system can provide not only information on the 3D distribution of particulate matter but also information on the particulate size distribution in a 3D space with the ability to convert this information to the standard EPA (Environmental Protection Agency) mass concentration units like  $PM_{10}$ ,  $PM_{2.5}$ , and  $PM_{1.0}$ .

Aerosol sounding techniques for the retrieval of physical aerosol parameters from multi-wavelength Lidar measurements have been developed since the 1980s and have made major progress in the past five years (Heintzenberg et al., 1981; Rajeev et al., 1998; Muller et al., 1999; Bockmann, 2001; Veselovskii et al., 2004). Unambiguous and stable retrieval of aerosol physical parameters requires measurements of backscatter coefficients at least at three laser wavelengths and aerosol extinction coefficients at least at two different wavelengths using additional Raman channels (Althausen et al., 2000; Bockmann, 2001). However, from the instrumental point of view, multi-wavelength Lidar systems with additional Raman channels are still very expensive and complicated to operate. Moreover, Raman signals are comparably weak and require significant integration time to achieve a reasonable signal to noise ratio to be useful for the retrievals (around 30-60 minutes for one measurement (Althausen et al., 2000)). Because of this, most Lidar systems with Raman channels typically operate at night to reduce background radiation from the atmosphere. For agricultural applications we need an inexpensive, robust and easily operated system that is able to provide particulate emission measurements in a matter of a few seconds under any meteorological and diurnal conditions and still be able to distinguish between different types of particulate emissions. A three-wavelength Lidar system appears to be a reasonable tradeoff between accuracy and stability of retrievals while providing the ability to operate under different environmental conditions with minimal measurement time. To date, a significant database of atmospheric aerosol characteristics has been obtained using a combination of satellite and ground based observations (Hess, 1998; Dubovik et al., 2002). Using this database, several researchers have shown that the physical properties of assumed aerosols can be successfully retrieved based on measurements of backscatter coefficients at only three wavelengths (Sasano et al., 1989; Rajeev et al., 1998; Del Guasta et al., 1994).

In this paper we present the initial results of the particulate emission characterization obtained by simultaneous remote measurements with a 3-wavelength Lidar system and in-situ point particulate measurements performed with standard EPA approved equipment. The combination of in-situ and remote measurements with the Lidar system pursues a twofold goal. First, particulate chemical and physical parameters measured in situ are used to make assumptions on the complex refractive index and type/shape of particle size distribution of particulate emissions present on the experiment site. In-situ measurements are also used to constrain the inverse solution to minimize overall errors and uncertainties in the Lidar measurements and the data analysis process. Second, in-situ measurements are used to calibrate and verify the results of Lidar retrievals. The experiment was conducted at the deep-pit swine production facility situated near Ames, in central Iowa, for approximately three weeks during August and September of 2005. An integrated system to measure whole facility emission was designed to characterize the complex structure and temporal/spatial variations in the particulate emission rates often associated with production operations (Bingham et al., 2006).

## 2. Experiment Setup and Overview of Employed Instrumentation

A schematic diagram of the deep-pit swine production facility and instrumentation employed on this site are shown in Figure 1.

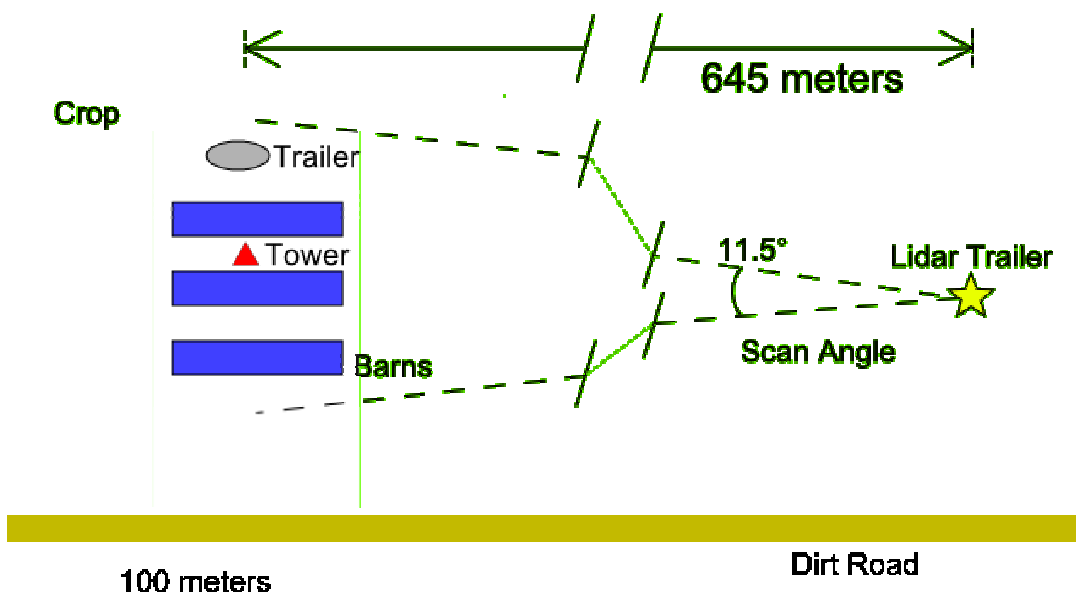


**Figure 1. Experimental site layout showing locations of in-situ sensors and the Lidar system**

The facility consisted of three separate, parallel barns, each of which housed around 1,250 pigs. The area around the facility was topographically flat and surrounded by fields of soybean and corn. A number of MetOne Optical Particle Counters (OPCs) 9722 were employed around this hog facility with units mounted at various heights on a tower erected at the center of the facility and a point source sensor trailer to provide information on particle size distribution continuously in real time. OPCs have the ability to count airborne particles in eight size ranges from 0.3 to 10  $\mu\text{m}$  in diameter, with sampling time of 20 sec. A pair of Tisch Cascade impactors at the central tower and sensor trailer provided filter-based particle size fractionation and concentration measurements in a range of 0.37-9  $\mu\text{m}$ . To measure chemical composition, real time particle ionic composition, and fine particle size distribution, the Aerodyne Aerosol Mass spectrometer (AMS) was deployed at the trailer. Portable  $\text{PM}_{10}/\text{PM}_{2.5}$  (AirMetrics MiniVol) samplers and passive  $\text{NH}_3$  (Ogawa Model 3300) samplers were arrayed vertically and horizontally around the three-barn production facility, and data were collected on a daily-averaged basis. The AirMetrics samplers were operated with  $\text{PM}_{2.5}$  impactor separation heads for approximately the first half of the field study and were then switched to the  $\text{PM}_{10}$  heads for the remaining portion of the study. A monitoring Davis weather station was established approximately 40 m to the north of the nearest barn to record the typical suite of meteorological parameters (wind speed, direction, temperature, etc.) for determination of near-source atmospheric advection and dispersion. A detailed description of the instrumentation and results of the in-situ measurements of particulate and gas emission are reported by Martin et al. in the proceedings of this Workshop.

The AGLITE Lidar instrument used in this study is a three-wavelength lidar system being designed and constructed at SDL under a contract with the ARS. A single diode-pumped Nd:YAG laser operating simultaneously at fundamental (IR-near infrared 1.064  $\mu\text{m}$ ), doubled (V-visible 0.532  $\mu\text{m}$ ), and tripled (UV-near ultraviolet 0.355  $\mu\text{m}$ ) frequencies is used as a transmitter of short impulses of radiation to probe scattering particles in the atmosphere. The high repetition rate of 10 kHz allows the use of low pulse energy for eye safe operations at the close ranges required for agriculture applications. The laser beam diameter is 10 mm, and beam divergence is approximately 0.2-0.3 mrad after beam-expanding optics. Outgoing laser energy is monitored by photo-sensors, and this information is transmitted to the data processing unit. The laser light backscattered from particles in the atmosphere is directed by a scanning mirror to a Newtonian telescope with a main-mirror diameter of 28 cm and a field of view (FOV) of 0.46 mrad. The beam-separation unit is used to split up the return backscattered light at three different channels according to wavelength. A photon counting detection system is chosen to detect low return signal simultaneously on

each channel. Interference filters are placed in front of each detector to suppress background daylight radiation from the atmosphere and optical cross talk between channels. The data from the photon counting unit are read out by a digital processing unit, averaged across a predetermined set of laser pulses, displayed in a real time, and stored and/or transmitted for further processing. The whole Lidar system was optimized for eye safe operation at all three wavelengths to allow full daylight operations at ranges from 0.5 to 15 km with a minimal range resolution of 5 m. Technical details of the Lidar design and construction are described by Wilkerson et al. in the proceedings of this Workshop.

The AGLITE Lidar system is trailer-mounted, and the scanning mirror is elevated above the trailer roof to provide a 270° azimuth by 45° elevation field of measurement. A digital camera co-aligned with the field of view of the Lidar and capturing imagery of the down-range scene is also mounted on the beam director. The AGLITE electronic control system automatically coordinates and synchronizes all the functions of the Lidar, scanning turret, data acquisition system, digital camera, and weather station to provide a complete data package and makes it available to the operator for further analysis. The Lidar trailer was placed at approximately 650 m east of the central tower (see Figure 1) and accompanied by a second weather station to monitor atmospheric conditions near the Lidar. This location of the Lidar system allowed full 3D volume measurements of particulate emissions from the three-barn feeding operations from a single observation point. Typical settings for the Lidar during operation are the following: accumulation time for return signal of 0.5-3 sec per measurement (5,000-30,000 laser pulses), range resolution of 5-15 m at ranges of 0.5-15 km, and azimuth and elevation scan speed of 0.05-2.0°/sec.

### 3. Inversion of the Lidar Signal to Retrieve Optical and Physical Properties of Aerosols

The Lidar return power from range R for two distinct classes of scatters may be written in the following form (Measures, 1984; Klett, 1985):

$$P(R, \lambda) = C \cdot \frac{P_0(\lambda)}{R^2} \cdot T^2(R, \lambda) \cdot [\beta_b(\lambda, R) + \beta_a(\lambda, R)] \quad (1)$$

Where  $C = \xi(R, \lambda) \cdot A_0 \cdot \Delta R = \xi(R, \lambda) \cdot A_0 \cdot \tau_d \cdot c/2$  is the Lidar calibration constant that includes losses in the transmitting and receiving optics  $\xi(R, \lambda)$  (Lidar overlap geometrical form factor), the effective telescope area  $A_0$ , and range increment  $\Delta R$  acquired by the Lidar that is defined by the detector integration pulse width  $\tau_d$  and speed of light  $c$ .  $P_0(\lambda)$  is a total laser power transmitted at wavelength  $\lambda$ .  $\beta_b(\lambda, R)$  and  $\beta_a(\lambda, R)$  stand for the backscatter coefficients of air molecules and aerosol particles, respectively.

Round trip laser beam transmittance along the beam pass  $T^2(R, \lambda)$  is defined by the equation:

$$T^2(R, \lambda) = \exp \left\{ -2 \int_0^R [\alpha_b(\lambda, R') + \alpha_a(\lambda, R')] dR' \right\} \quad (2)$$

Where  $\alpha_b(\lambda, R)$  and  $\alpha_a(\lambda, R)$  are extinction coefficients of air molecules and aerosols, respectively.

Retrieval of aerosol physical parameters from a raw Lidar signal involves four major steps:

- 1) Account for geometrical form factor of the telescope receiving optics and scattered sunlight background radiation. The geometrical form factor in equation (1) takes into account the overlap between the transmitted laser beam and the FOV of the telescope receiving optics with the central obstruction and can be estimated theoretically (Measures, 1984). In real life, this factor can change after setup of the portable Lidar system in the field, and the real geometrical form factor  $\xi(R, \lambda)$  shall be determined experimentally. To calculate the geometrical form factor at field conditions, the polynomial regression method for an inhomogeneous atmosphere proposed by Dho et al., 1997 is used. This method does not require special atmospheric conditions and in many cases can be used during operational field measurements. During daylight observations the background radiation of sunlight scattered by the atmosphere dominates the Lidar return signal at long distances. For each Lidar measurement this background radiation is approximated by least

squares fitting to a constant value at distances of 13-15 km and then subtracted from the total Lidar return signal.

- 2) Calculate the optical parameters (backscatter and extinction coefficients) of the background aerosols and particulate emission from the feeding facility at three wavelengths, utilizing Klett's analytical solution for two scattering components (Klett, 1985). Typically, the molecular part of equation (1) can be calculated using standard atmosphere conditions at different altitudes and the well known and parameterized refractive index, backscatter and extinction properties of the air molecules (Bockmann, 2004). Aerosol backscatter and extinction coefficients remain two unknowns in a single Lidar equation that describes one particular Lidar measurement. We are using the standard solution of this equation proposed by Klett that involves a priori assumption of the relationship between aerosol extinction and backscatter coefficients that is usually called the Lidar ratio L:

$$L_a = \alpha_a(\lambda, R) / \beta_a(\lambda, R) \quad (3)$$

Another assumption deals with selecting a boundary value to determine the constraint factor required by Klett's solution, usually a calibration or reference value of the extinction coefficient  $\alpha_{aD} = \alpha_{aD}(\lambda, R_D)$  independently measured at a certain distance  $R_D$ .

The original solution of equation (1) has been deducted for typical atmospheric applications when the Lidar system is looking straight up so that molecular contribution is significant for altitudes above the aerosol boundary layer (ABL). For agricultural applications all measurements are conducted close to the ground, and the main contribution to atmospheric scattering is determined by aerosols while the molecular contribution is negligibly small. In this case we are still dealing with two distinct types of scatterers such as background aerosols and airborne particulate matter emitted from the agricultural activities. For this application, the original solution of equation (1) is still valid, and we attribute the subscript "b" to the atmospheric background aerosols while the subscript "a" will refer to the particulate emission. Typically the agricultural particulate emission is spatially localized around the emission source while the rest of the Lidar signal is dominated by the surrounding background aerosols. In close proximity to the emission source the background aerosol loading is typically homogeneous, and a standard slope method (see for instance Klett, 1985) can be applied to retrieve the extinction coefficient of the background aerosols. For each wavelength, the slope of a line that has been fit in a least-squares sense to the curve  $S(R) = \ln[P(R, \lambda) \cdot R^2]$  presents nearly a straight line.

- 3) Estimate parameters of particle size distribution for background aerosols and particulate emission using an iterative technique to minimize the difference between simulated (Mie theory) and measured extinction coefficients at three Lidar wavelengths.

Based on the OPC data measured in situ, we approximate the particle size distribution by a bimodal distribution, using the standard Power law function for the accumulation mode:

$$n(r) = N_1 r^v \quad (4)$$

and lognormal size distribution for the coarse particle mode:

$$n(r) = \frac{1}{r} \frac{N_2}{(2\pi)^{1/2} \cdot \ln \sigma} \cdot \exp\left[-\frac{(\ln r - \ln r_m)^2}{2 \cdot \ln^2 \sigma}\right] \quad (5)$$

Where  $N_1$  is a constant related to the total number of particles with radius  $r$  in accumulation mode and  $v$  is the size index that generally varies in a range of 3-5.  $N_2$  represent the total density of particles in the coarse mode with mode radius of  $r_m$  and width of distribution  $\sigma$ .

To estimate the mode radius and particle number densities  $N_1$  and  $N_2$ , we are using a modified version of the minimization technique described by Del Guasta (1994). The minimization function in our case is constructed on the differences between the extinction coefficients  $\alpha_i$ , retrieved from the Lidar signal, and  $\alpha_i^{calc}$ , calculated using Mie theory (Bockman, 2001) at three laser wavelengths. Arbitrary values of the Lidar ratio for both background aerosols  $L_b$  and particulate

emission  $L_a$  are assumed initially at step 2. Estimated particle size distributions in step 3 are used to update these values through Mie calculations. Steps 2 and 3 are then repeated iteratively to achieve a minimal value of the minimization function.

- 4) Calculate volume concentration and convert it to the mass concentration using in-situ chemical and physical property measurements. Once the parameters of particle size distribution and number densities are estimated, the mass concentration of particles with different size ranges can be easily calculated using in-situ measurements of particulate chemical composition and density (Hinds, 1998).

#### 4. Experimental Results and Discussion

An extended series of Lidar observations were conducted during three weeks of field campaign at the deep-pit swine production facility. Most of measurements were conducted at day and night time to capture the dynamic of particulate flux emission from the production facility. The local climate was typically characterized by clear skies, and winds were generally mild at 0-3 m/s, changing direction from west to south during the study period. Typical Lidar scan patterns include vertical scans between barns and on any side of the barns and sensor trailer, horizontal scans above the barns at any chosen elevation, stationary time series scans of particulate emission in close proximity to the in-situ instrumentation, and any combination of vertical and horizontal scans to capture and monitor 3D distribution and variation of the particulate emission. Depending on the prevailing wind conditions, the measured profiles of particulate emission varied significantly from day to day and occasionally even hour to hour.

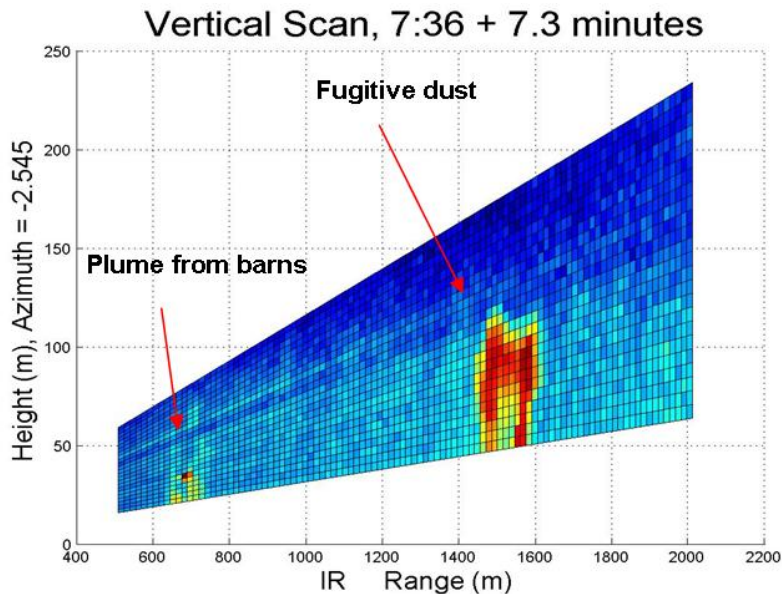


**Figure 2. Vertical Lidar scan measured at  $\lambda=1.064 \mu\text{m}$  near the central tower on 09/02/05, 7:36 am under still weather conditions**

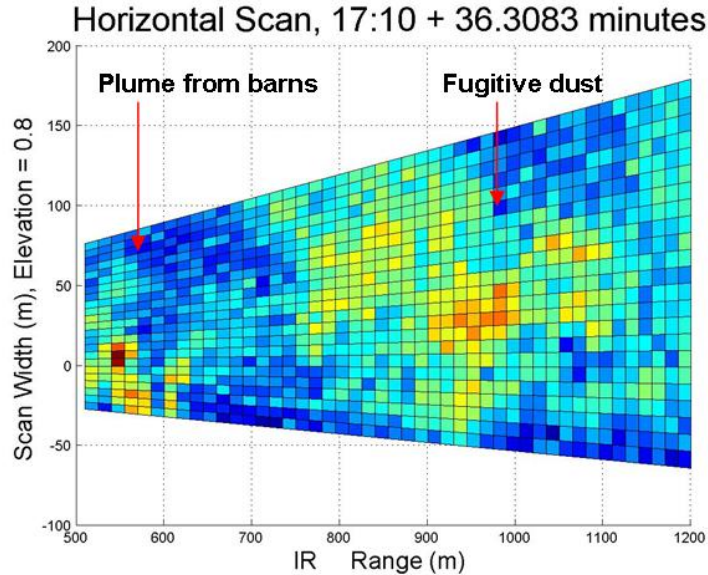


**Figure 3. Horizontal Lidar scan measured at  $\lambda=1.064 \mu\text{m}$  on the elevation of  $\sim 5\text{m}$  above the barns on 09/01/05, 5:10 pm under west wind of 3 m/s.**

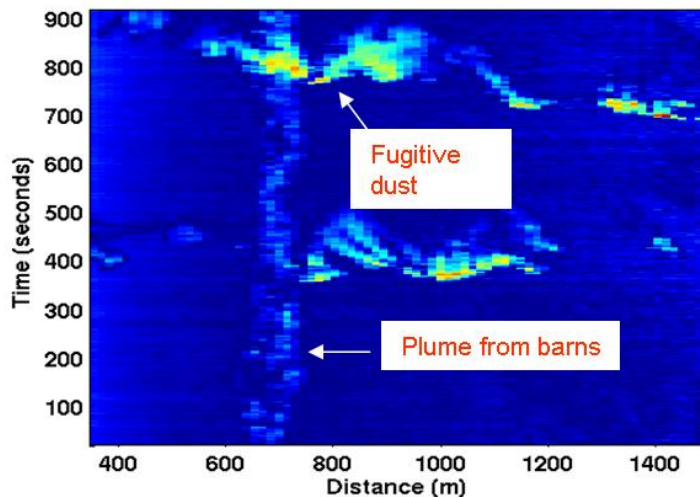


**Figure 4. Time series of pollutant and fugitive dust emissions measured at  $\lambda=1.064 \mu\text{m}$  under south wind conditions when Lidar is pointing at the middle of the tower.**

Two dirt roads were bordering the swine production facility. One road ran east to west at a distance of  $\sim 115$  m south from the central measurement tower. The second road ran north to south at a distance of  $\sim 900$  m west from the tower. Occasional traffic along both roads caused extensive fugitive dust traveling from roads over the swine facility. These events were captured as well during Lidar operations. Examples of vertical, horizontal, and pointed (time series) Lidar scans are shown in Figures 2, 3, and 4 respectively.

These images are rendered in false color where the color represents the intensity of semi-processed Lidar return signals with background radiation from the sun and background aerosols removed. In all images the particulate emission from the barns is clearly distinguished from the fugitive road dust due to separation of these events in space and time. The particulate emission from barns was localized between barns at a distance of  $\sim 650$  m from the Lidar (the location of the central measurement tower), while fugitive dust clouds (Figures 2 and 3) were coming from the western road located at a distance of  $\sim 1550$  m from the Lidar. The vertical scan in Figure 2 was measured at a still wind condition so that both the fugitive dust cloud and the particulate emission were spatially localized around the emission sources expanding upward

due to convective turbulence. The horizontal scan in Figure 3 was taken under west wind conditions, and the data show that both particulate emission and fugitive dust were swept by the wind toward the Lidar and extended horizontally as compared to Figure 2. The time series in Figure 4 was measured under south wind conditions when fugitive dust was blown from the south road, which was parallel to the line of Lidar range measurements. A weaker signal at a range of  $\sim 650$  m represents particulate emission between swine barns measured at a height of  $\sim 6$  m in a close proximity to the OPC sensor mounted on the tower.

Due to the spatial and temporal separation of different particulate emissions in the return Lidar signal, these events can be easily processed separately so that optical and physical properties of particulate emissions from different sources can be extracted using single Lidar scan. For all cases the return signals from fugitive dust clouds were about an order of magnitude stronger than the signal from barn particulate emissions, which in some cases only slightly exceeded Lidar returns from the background aerosols in the air surrounding the facility. The retrieval procedure briefly described in a previous section was tested on both cases, for which there are remarkably different physical origins of particulate emissions involved.

Proper conversion of Lidar data involves the construction of a model for the particulate composition and size distribution based on in-situ measurements. Following the OPAC database (Hess, 1998) we assumed that fugitive dust is composed of a mixture of quartz and clay materials. Particle size distribution was approximated by a bimodal distribution based on in-situ measurements with OPC sensors. The results of the retrievals are shown in Figure 5. Extinction coefficients retrieved at three laser wavelengths in step 2 are shown in Figure 5A as a function of the distance from Lidar. The dust cloud chosen for conversion is extended for almost 1 km from the west road toward Lidar and shows different ratio of extinction coefficients measured at different wavelengths. As a result, the parameters of particle size distributions estimated at different distances are different, which leads to a different ratio of small (accumulation mode) and large (coarse mode) particles within the same dust cloud.

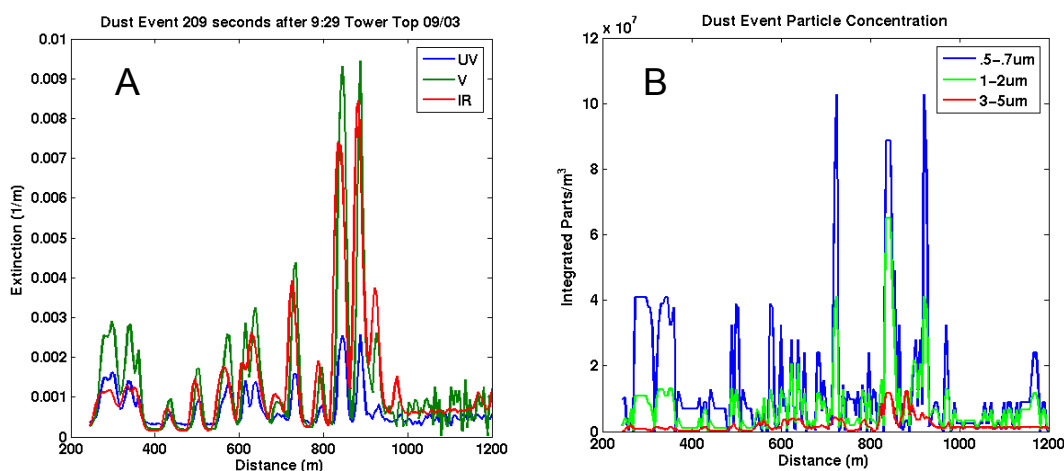


**Figure 5. Optical and physical properties of fugitive dust cloud retrieved from the Lidar signal at different distances from the Lidar. A) Extinction coefficient at three Lidar wavelengths. B) Volume concentrations for dust particles with radius range of 0.5-0.7  $\mu\text{m}$ , 1-2  $\mu\text{m}$ , and 3-5  $\mu\text{m}$  estimated from extinction coefficients.**

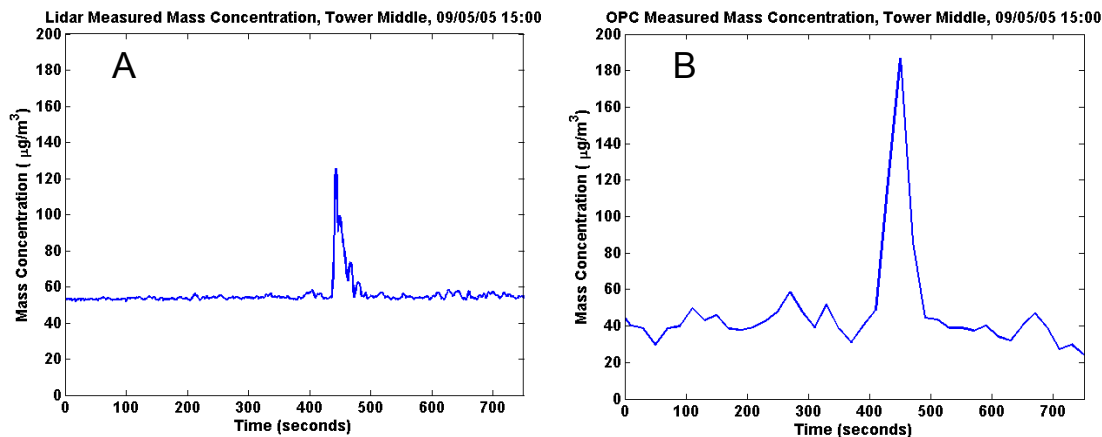


**Figure 6. Time series of dust particles mass concentration  $PM_{10}$  as measured by the Lidar (graph A) and OPC sensor mounted on the top of the tower (graph B). Measurements are collocated in time and space.**

Volume concentrations of particles with radiuses in a range of 0.5-0.7  $\mu\text{m}$ , 1-2  $\mu\text{m}$ , and 3-5  $\mu\text{m}$  were calculated from size distributions estimated in the retrieval step 3 and are shown in Figure 5B. It is seen that the large particle concentration decreases while the concentration of small particles increases with the distance from road along the wind, showing settlement of large particles from the dust cloud.

Mass concentration  $PM_{10}$  estimated from the Lidar signal is compared with in-situ measurements by OPC in Figure 6. Both measurements represent a time series of particulate emission measured simultaneously at the top of the tower, where the peak concentration represents a fugitive dust event and the base signal is mostly due to the background aerosols. Concentration of background aerosols and fugitive dust from the road measured by the Lidar are both in good quantitative agreement with coincident OPC measurements.

As mentioned previously, particulate emissions from the swine facility only slightly exceed the background aerosol loading. Lidar returns are still sensitive to these small variations, which can be easily spotted due to their spatial localization in the return Lidar signal. The OPC sensors provide continuous point measurements so that background aerosols and particulate emission can be distinguished only by the numbers of counts (intensity of the signal). Comparison of the OPC data measured between barns and far away from barns where only background aerosol is present shows that particulate emission counts are on the level of natural variability of the background aerosol loading. In this case it is difficult to extract exact information on the particulate size distribution from the OPC data. Taking this into account, we also approximated the particulate size distribution by a bimodal distribution, as in a case of fugitive dust and background aerosols. Preliminary chemical analysis of the particulate emission measured in situ (Martin, 2006) shows that its composition may be considered as a standard water soluble aerosol mixture composed from various kind of sulfates, nitrates, organic carbon, etc. (Hess, 1998). Assuming these approximations, Lidar returns from a particulate plume were processed and parameters of particulate size distribution were estimated as described in section 3. Once parameters of particle size distribution are estimated, the mass concentration of  $PM_{2.5}$  is calculated assuming an average particle density of 1.8  $\text{g}/\text{cm}^3$ . The results of these calculations are shown in Figure 7 for two time series of Lidar measurements pointed at the middle of the tower and at its top.

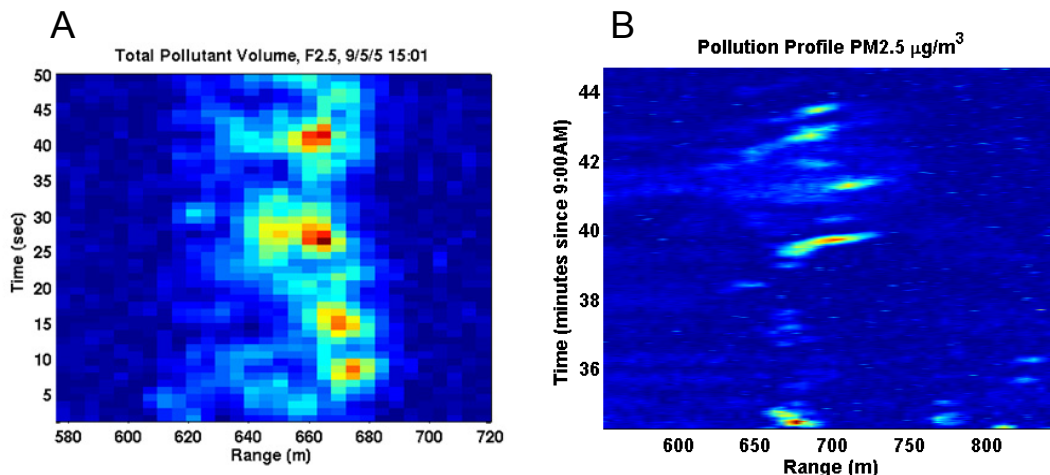


**Figure 7. Comparison of the PM<sub>10</sub> concentration at the middle of the tower (A) and at the tower top (B) as estimated from the Lidar returns.**

It is interesting to note that particulate was emitting from barns as periodical events with periodicity of 3-10 seconds as can be seen in both images of Figure 7. During these observations the Lidar accumulation time was set to 1 second, and that was enough to resolve the periodic nature of particulate emission. The accumulation time of OPC monitoring sensors was 20 seconds so that OPC counts represent a time average of periodic events that contributed to the inability of OPC sensors to resolve clearly particulate emissions and background aerosols.

Preliminary comparisons of the Lidar retrievals with in-situ PM<sub>2.5</sub> measurements shows that total PM<sub>2.5</sub> mass concentration agrees within an order of magnitude.

## 5. Conclusion

A three-wavelength portable scanning Lidar system has been developed at SDL to derive information of particulate spatial distribution and optical/physical properties of aerosols over remote distances using an instrument located at a single convenient point. Preliminary results discussed in this paper show the great potential of remote Lidar measurements to quantitatively characterize particulate emission from different sources. Lidar technology represents a unique technique to characterize spatial and temporal variations of particulate emission from any source met in field conditions. Additionally, the high measurement rate of the Lidar allows us to capture temporal variations in particulate emissions on the order of seconds that could not be resolved by most in-situ point instrumentation. The use of extinction/backscatter ratios derived from Lidar measurements at three laser wavelengths was found to be a promising method for remote measurements of the size distribution of particulate emissions present in the field. These emissions include background aerosols, emissions from the feeding facility, and fugitive dust from the road. The strength of Lidar returns from these sources varies by an order of magnitude, and the inversion algorithm developed to process three wavelength Lidar data gives meaningful results for all sources of particulate emissions. Retrieval results for fugitive road dust are in a good agreement with coincident in-situ measurements by OPC sensors. The retrievals of mass concentration of particulate emission from the feeding operation agree on the order of magnitude with in-situ measurements performed with PM<sub>2.5</sub> ambient samplers. The main uncertainties involved in such a method are due to the incomplete knowledge of the particulate refractive index and parameters of particle size distribution to further constrain the iterative minimization technique employed in this method to estimate parameters of assumed size distribution. Further work is needed for both remote Lidar and in-situ point measurements to verify, calibrate, and correlate all types of measurements performed in the field.

## References

Althausen D., D. Muller, A. Ansmann, U. Wandinger, H. Hube, E. Clauer, and S. Zorner. 2000. Scanning six-wavelength eleven channel aerosol lidar. *J. Atmos. Ocean. Technol.* 17: 1469–1482.

- Bingham G. E., J. Hatfield, J. H. Prueger, T. D. Wilkerson, V. V. Zavyalov, R. L. Pfeiffer, L. Hipps, R. Martin, P. Silva, W. Eichinger. 2006. An Integrated Approach to Measuring Emissions from Confined Animal Feeding Operations at the Whole Facility Scale. Proceedings of the Workshop on Agricultural Air Quality: June 5-8.
- Bockmann C. 2001. Hybrid regularization method for ill-posed inversion of multiwavelength lidar data in the retrieval of aerosol size distributions. *Appl. Opt.* 40: 1329–1342.
- Bockmann C. , U. Wandinger, A. Ansmann, J. Bosenberg, V. Amiridis, A. Boselli, A. Delaval, F. De Tomasi, M. Frioud, I.V. Grigorov, A. Hagard, M. Horvat, M. Iarlori, L. Komguem, S. Kreipl, G. Larcheveque, V. Matthias, A. Papayannis, G. Pappalardo, F. Rocadenbosch, J. A. Rodrigues, J. Schneider, V. Shcherbakov, and M. Wiegner. 2004. Aerosol lidar intercomparison in the framework of the EARLINET project. 2. Aerosol backscatter algorithms. *Appl. Opt.* 43: 977-989.
- Del Guasta M., M. Morandi, L. Stefanutti, B. Stein, and J. P. Wolf. 1994. Derivation of Mount Pinatubo stratospheric aerosol mean size distribution by means of a multiwavelength lidar. *Appl. Opt.* 33: 5690–5697.
- Dho S. W., Y. J. Park, and H. J. Kong, 1997. Experimental determination of a geometrical form factor in a lidar equation for an inhomogeneous atmosphere. *Appl. Opt.* 36: 6009-6010.
- Dubovik O., B. Holben, T. F. Eck, A. Smirnov, Y. J. Kaufman, M. D. King, D. Kino, D. Tanre, and I. Slutsker. 2002. Variability of absorption and optical properties of key aerosol types observed in worldwide locations. *J. Atm. Scie.* 59: 590-608.
- Heintzenberg J., H. Muller, H. Quenzel, and E. Thomalla. 1981. Information content of optical data with respect to aerosol properties: numerical studies with a randomized minimization-search-technique inversion algorithm. *Appl. Opt.* 20: 1308–1315.
- Hess M., P. Koepke, and I. Schult. 1998. Optical Properties of Aerosols and Clouds: The software package OPAC. *Bull. Am. Meteorol. Soc.* 79: 831-844.
- Hinds W. C. 1998. *Aerosol technology. Properties, behavior, and measurement of airborne particles.* John Wiley & Sons, Inc., New York.
- Hipps L.E. and D.F. Zehr. 1995. Determination of evaporation from integrated profiles of humidity and temperature over an inhomogeneous surface. *Boundary-Layer Meteorol.* 75: 287- 299.
- Klett J. D. 1985. Lidar inversion with variable backscatter/extinction ratio. *Appl. Opt.* 24: 1638-1683.
- Martin R.S., V. Doshi, and K. Moore. 2006. Determination of Particle (PM10 and PM2.5) and Gas-Phase Ammonia (NH3) Emissions from a Deep-Pit Swine Operation using Arrayed Field Measurements and Inverse Gaussian Plume Modeling. Proceedings of the Workshop on Agricultural Air Quality: June 5-8.
- Measures R. M. 1984. *Laser remote sensing: Fundamentals and applications.* John Wiley & Sons, Inc., New York.
- Muller D., U. Wandinger, and A. Ansmann. 1999. Microphysical particle parameters from extinction and backscatter lidar data by inversion with regularization: theory. *Appl. Opt.* 38: 2346–2357.
- Rajeev K. and K. Parameswaran. 1998. Iterative method for the inversion of multiwavelength lidar signals to determine aerosol size distribution. *Appl. Opt.* 37: 4690–4700.
- Sasano Y. and E. V. Browell. 1989. Light scattering characteristics of various aerosol types derived from multiple wavelength lidar observations. *Appl. Opt.* 28: 1670-1679.
- Veselovskii I., A. Kolgotin, V. Griaznov, D. Muller, K. Franke, and D. N. Whiteman 2004. Inversion of multiwavelength Raman lidar data for retrieval of bimodal aerosol size distribution. *Appl. Opt.* 43: 1180-1195.
- Wilkerson T.D., G. E. Bingham, V. V. Zavyalov, J. A. Swasey, J. J. Hancock, B. G. Crowther, S. S. Cornelsen, C. Marchant, J. N. Cutts, D. C. Huish, C. L. Earl, J. M. Andersen, and M. L. Cox. 2006. AGLITE: A Multiwavelength Lidar for Aerosol Size Distributions, Flux and Concentrations of Whole Facility Emissions. Proceedings of the Workshop on Agricultural Air Quality: June 5-8.



## Particulate Matter Emissions from an Ohio Belt-Battery Layer Barn

L.Y. Zhao<sup>1</sup>, T.T. Lim<sup>2</sup>, A.J. Heber<sup>3</sup>, H. Sun<sup>4</sup>, C.A. Diehl<sup>5</sup>, J.-Q. Ni<sup>6</sup>, P.C. Tao<sup>7</sup>, and S.M. Hanni<sup>7</sup>

<sup>1</sup>Assistant Professor, <sup>4</sup>Research Associate, The Ohio State University, Columbus, OH 43210

<sup>2</sup>Research Scientist, <sup>3</sup>Professor, <sup>5</sup>Research Engineer, <sup>6</sup>Technical Director, and <sup>7</sup>Reserch Assistant, Purdue University, West Lafayette, IN 49707

### Abstract

Particulate matter (PM) emissions from concentrated poultry laying houses cause significant environmental and health concerns. Quantifying and characterizing PM emissions and effectiveness of mitigation technology for layer facilities will allow the poultry industry to control the particulate emissions more effectively. This study assessed PM emissions from a new belt-battery laying facility through six months of continuous measurement. PM<sub>10</sub> concentration was continuously measured by using the Tapered Element Oscillating Microbalance (TEOM) system. Gravimetric samplers were used to sample total suspended particulate matter twice per week. Barn ventilation was estimated via field tests and continuous monitoring of fan control signals, vibration, and differential static pressure of all fans. The average daily mean (ADM) concentration of PM<sub>10</sub> and TSP were 265±108 µg/dsm<sup>3</sup> and 3070±675 µg/dsm<sup>3</sup> at the barn exhaust locations, respectively. The ADM emission rates of PM<sub>10</sub> and TSP from the belt battery layer barn were 20±18.9 mg/d-hen and 168±110 mg/d-hen, respectively. Based on these emission rates, 13.7 million hens would emit 100 tons of PM<sub>10</sub> and 4.1 million hens would emit 250 tons of TSP per year, respectively. The PM<sub>10</sub> concentration in the manure belt battery layer barn was only 45-53% of that in high-rise barns. PM<sub>10</sub> emission rate of the belt battery barn was only about 62% that of the high-rise barns. Similar levels of TSP concentrations and emission rates in the manure belt battery barn were measured in comparison with the high-rise deep-pit layer barns.

### Introduction

Air emissions from animal production facilities have caused public concern about human health, animal health, and the global environment (NRC, 2003). Dust particles carry odor, gases, and bacteria and therefore are of the greatest health concerns. In poultry buildings, the combination of dust and other air contaminants such as ammonia may cause respiratory disease, increased mortality rates, and reduced bird growth (Maghirang et al. 1991).

PM emissions are directly regulated under the Clean Air Act (CAA) in terms of ambient PM concentrations and emission thresholds for major emission sources. Among animal production facilities, poultry facilities create the most concern with regard to emitting the amounts of PM that could potentially violate CAA (Heber, 2004). Dust and ammonia emissions have created a major challenge for the viability and growth of the egg-laying industry. Therefore, understanding and controlling PM emissions to sustain the viability and growth of the poultry industry is of utmost importance. However, scientific data on PM emissions from poultry facilities are limited. Such insufficient scientific data has hindered the development of PM control technologies and effective management practices in the poultry industry. Collecting reliable emission data and accurately assessing PM control technologies and practices have become necessities.

Particulate emissions from poultry buildings were studied by European researchers at 81 poultry facilities in four countries over a 24-hour period in each of two seasons (Takai et al., 1998). This short term study showed that the mean inhalable and respirable dust emission rate from caged layer facilities with manure belts and deep pit were in the range of 398-872 and 24-161 mg/h-AU (AU=500 kg live weight), respectively. Statistically significant (p<0.001) effects of housing facilities on dust emissions were revealed. Lim et al. (2003) continuously studied PM concentrations and emissions of a representative US deep-pit laying hen house by using the microweighing (TEOM) and real-time ventilation monitoring technologies to determine variations of PM emissions during a 12-month period. Heber et al. (2005) has intensively quantified continuous baseline emissions of PM<sub>10</sub> and TSP from a high-rise deep-pit poultry layer barn over a fifteen month period.

In the U.S., high-rise deep-pit and manure belt laying facilities account for 73% and 23% of current laying hen production, respectively. The manure belt laying facilities are considered a newer facility design and account for 60% new facilities (Xin, 2005). Ammonia emission rates from the manure belt laying facilities range from 0.054-0.094 g / d-hen, significantly lower than that from traditional high-rise deep-pit laying facilities which ranges from 0.83-0.90 g/d-hen (Liang et al., 2005). Sun et al. (2005) confirmed significant ammonia mitigation effects of a manure belt battery laying facility through a continuous six-month measurement.

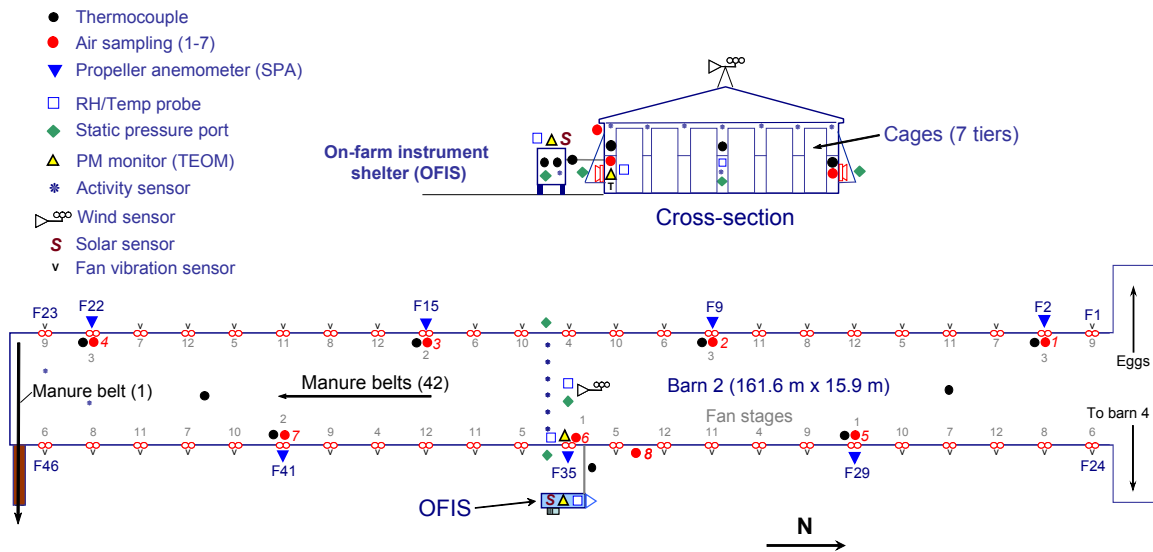
Nevertheless, the effects of the new manure belt laying facility on PM emissions have not been scientifically documented. Quantifying PM emissions from the new manure belt layer facilities will supply the poultry industry with vital information in the adoption of new facilities and the control of ammonia and PM emissions. Thus, improvement of air quality and compliance with federal air quality laws will be facilitated. The objective of this study was to quantify PM emissions from a belt-battery laying facility.

### **Materials and Methods**

One commercial manure belt-battery layer house (MB barn) located in central Ohio was monitored for this study. On August 10, 2004, continuous PM emission measurements began to be conducted and continued for six months. Emission rates of particulate matter with an aerodynamic diameter equal or smaller than 10 micro (PM<sub>10</sub>) and total suspended particulate (TSP) were measured. A mobile air quality lab was used to host equipment and data acquisition systems. Tapered Element Oscillating Microbalances (TEOMs) were used to continuously monitor PM<sub>10</sub> concentrations of the building's exhaust air and ambient air. Total suspended particulate concentration was measured periodically using a TSP gravimetric sampler. Barn ventilation and indoor environment was continuously monitored. Emission rates of TSP and PM<sub>10</sub> were calculated by multiplying concentrations by total barn ventilation airflow rates.

#### **Layer Barns**

The MB barn had been converted from an old high-rise deep-pit barn in 2004. On the same site, another 15 barns were also in differing stages of the process of being converted from high rise barns to manure belt battery barns. The barns were oriented from north to south and were spaced 15.9-m apart. The barn used in the study was 161.6 m long x 15.9 m wide and housed approximately 168,000 hens in six rows of 7-tier crates. Figure 1 shows the schematic of the barn and sampling locations. Manure was collected on plastic belts under the cages and removed from the barn within 1 to 7 days. Air was blown on the belt to reduce manure moisture content. Continuous slot inlets over the top of each row of layer cages introduced fresh air from the attic into the barn and forty-six 122-cm belted axial fans (Model GP48G600MNA, S.N. REVA 4-04, ValAir, 2599 Old Philadelphia Pike, Bird 'N Hen, PA 17505) installed uniformly on the two side walls along the barn length exhausted the dirty air out of the barn. The fans in the barn were 6.4 m apart. The barn had 12 temperature sensors and was ventilated in 12 stages. Each stage consisted of four fans, except for stages 1 and 2, which have 3 fans each. Eggs are removed on conveyors into the egg processing plant. The lights are shut off from 8:00pm to 4:00am each night. Egg production along with water and feed consumption were recorded automatically, and daily mortalities were recorded manually.

**Figure 8. Schematic of the belt battery layer barn and sampling locations**

### Measurement of Particulate Matter Concentration

The PM<sub>10</sub> concentrations were continuously measured using the commercially available equipment, TEOM 1400a Ambient Particulate (PM<sub>10</sub>) Monitor (Rupprecht & Patashnick, Albany, NY). The TEOM PM<sub>10</sub> measurement method was designated by the USEPA as an equivalent method (EPA Designation No. EQPM-1090-079). The TEOM equipment with PM<sub>2.5</sub> inlet is also used extensively in state and national PM<sub>2.5</sub> monitoring networks. The TEOM monitor is designed for ambient air monitoring, indoor air quality assessment, and exposure studies. The key to the device is a tapered element oscillating microbalance, which is an inertial mass measurement technique for making a direct measurement of the particle mass collected on a filter in real time. The device operates at an industry-standard, volume-controlled flow rate of 16.7 L/min. It can be outfitted with a variety of commercially available pre-separator inlets suitable for measuring TSP, PM<sub>10</sub>, and PM<sub>2.5</sub> (Heber et al., 2002). The TEOM sampling head was placed near an exhaust fan and in a relatively low speed air stream. The TEOM pumps and controllers were stationed in the instrument shelter and provided vacuum to the filters via long vacuum tubes. The sample stream temperature was maintained at 50°C. The PM concentrations measured by the TEOMs were adjusted to report data at one atmosphere pressure (1 atm) and 20°C.

A three-point TSP gravimetric sampler (Wang et al, 1999) was used to collect TSP dust samples. The TSP dust sampler consisted of an isokinetic sampling head, a 37 mm diameter glass fiber filter (Millipore, 0.7- $\mu$ m pore size), 37-mm diameter filter holder (Millipore Aerosol Analysis Monitor), 1.57 mm dia. critical venturi orifice, plastic tubing, and an electric air pump (Gast, model 1023-V131Q-G608X). The dust sampler was run 24 to 72 h to account for the changing PM levels over the course of one to three working days. The sampling heads were located at three different heights in front of an exhaust fan inlet (less than 0.5 m from the fan impellers). The locations of TSP sampling heads were carefully selected by using a portable vane thermoanemometer (Model 451126, Extech, Bohemia, NY), which matched the 2 m/s airflow speed required for isokinetic sampling. The filters, both new and dusty, were desiccated for 24 h before and after weighing. Acetone was used to rinse dust remnants off the sampling heads. PM concentration was calculated by dividing total PM mass collected by air volume sampled.

### Ventilation and Barn Environment Measurement

Differential pressures were monitored continuously in the barns near the exhaust fans by using differential pressure transmitters (Model 2671-100-LB11-9KFN, Setra, Boxborough, MA) with a range of  $\pm 100$  Pa and an accuracy of  $\pm 0.5$  Pa. Atmospheric pressures were monitored with barometric pressure transducers in the TEOMs.

The operating status (on/off) of each fan stage was monitored via auxiliary contacts of fan motor control relays. Fan airflow capacities were measured in the field with a fan airflow numeration system (FANS) and a portable fan tester (Gates et al. 2004). Also, at the University of Illinois, fan airflow capacities were calibrated at an accuracy within 2% by using a fan test chamber. In addition, the operating status of each fan was individually monitored via vibration sensors (Ni et al., 2005).

The temperature of exhaust air was monitored using copper-constantan thermocouples (Type T). An electronic relative humidity (RH) and temperature transmitter (Model HMW61, Vaisala, Woburn, MA) was used to monitor temperature and relative humidity at a representative exhaust location in the barn.

### Calculation of PM Emission Rates

PM emission rates were simply calculated as the product of PM concentration multiplied by barn ventilation airflow rate. Ventilation rate was adjusted to the standards if 1 atmospheric pressure and 20°C. Equation 1 was used for TSP emission calculation. Equation 2 was used for TEOM PM<sub>10</sub> emission calculation.

$$E = QC \quad (1)$$

$$E = Q \frac{293}{(273 + T)} \frac{P}{P_0} C_0 \quad (2)$$

Where:

E	PM gross emission rate, µg/s
Q	Exhaust airflow rate at T, m <sup>3</sup> /s
P	Pressure of exhaust air, atm
P <sub>0</sub>	Standard pressure, 1 atm
C <sub>0</sub>	PM concentration or concentration difference measured by TEOM(s), µg/m <sup>3</sup>
T	Temperature of exhaust air, °C

The gross emission rates were calculated directly from exhaust PM<sub>10</sub> concentrations multiplied by airflow rates. The net emission rates were calculated using the difference of exhaust PM<sub>10</sub> concentrations and monthly average of ambient PM<sub>10</sub> concentrations multiplied by barn airflow rates.

### Data Analysis

General statistical data analysis was conducted initially to calculate average daily means (ADM) with 95% confidence interval and standard deviations of each measurement parameters. A two-way analysis of variance (ANOVA) with a complete randomized block model was used to analyze statistical differences of PM emission rates during light hours and dark hours and in winter months from the BB barn and two high-rise deep-pit barns (HR). Paired t-test analysis was used to compare PM emission rates from the BB barn and two HR barns. The statistical significance level of 0.05 was used to judge whether the statistical hypothesis (there is no statistical difference) should be rejected (P<0.05) or not (P>0.05).

### Results and Discussion

The reported results are average daily means. Basic statistics of the data were analyzed and the data were validated through cross-checking other condition parameters. With over 70% valid data, it is reasonable to conclude that these results have avoided the bias that can be caused by insufficient data.

### Indoor Environment of the Barns

Daily mean barn temperature, RH, and ambient temperatures are presented in Figure 2. During the test period from Aug. 2004 to Jan. of 2005, daily average ambient temperature dropped from 26.2°C to -13.7°C with an overall average outdoor air temperature of 10.6 °C. The testing period covered hot, mild, and cold seasons. The ADM barn temperature was 20.8 °C at the middle tier cages and 22.9 °C at the barn exhausts. Since exhaust fans are located uniformly on two side walls and liner slot air inlets are located on the tops of each row of cages, the cold fresh air picked up heat, moisture and air emissions from hens as well as manure exhausted through the exhaust fans. Therefore, ADM temperature at the center middle tier cages was lower than that at the exhaust fans. The indoor temperature was slightly higher on hot days and slightly

lower on cold days. Overall however, the barn temperatures were maintained relatively stable across seasons.

Daily mean RH of exhaust air ranged from 45 to 80% with an average RH of  $60 \pm 6.4\%$ . The ambient RH ranged from 48% to 98% with an average RH of  $72 \pm 11\%$ . Since the barn was not equipped with any cooling system, when outdoor RH and temperature were high in August and early September of 2004, the average indoor RH averaged  $67 \pm 6.7\%$ , which was much higher than the average RH of October to January, which was  $58 \pm 5\%$ . Therefore, the indoor RH fluctuated much more widely than did the indoor temperature.

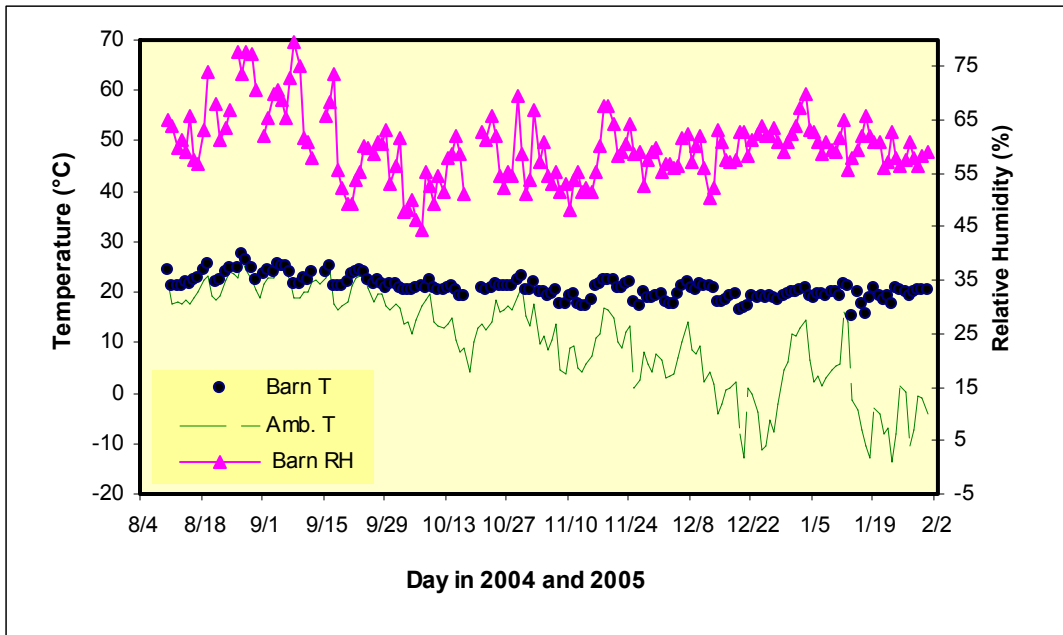


**Figure 2. Daily mean temperature and relative humidity of the belt-battery barn**

Figure 3 shows the building differential pressures and ventilation rates. The daily mean pressures were maintained at about -20 Pa with small fluctuations most of the time. In January, due to ice built up on the baffled air inlet and a small number of running fans, large static pressure fluctuations of about  $\pm 10$  Pa was observed. Affected by weather conditions, barn ventilation rates were higher in hot August and lower in cold January. Daily mean ventilation rates ranged from 26 to  $337 \text{ dsm}^3/\text{s}$  with an average of  $129 \pm 98 \text{ dsm}^3/\text{s}$ . Ventilation rate fluctuated significantly on hot days.

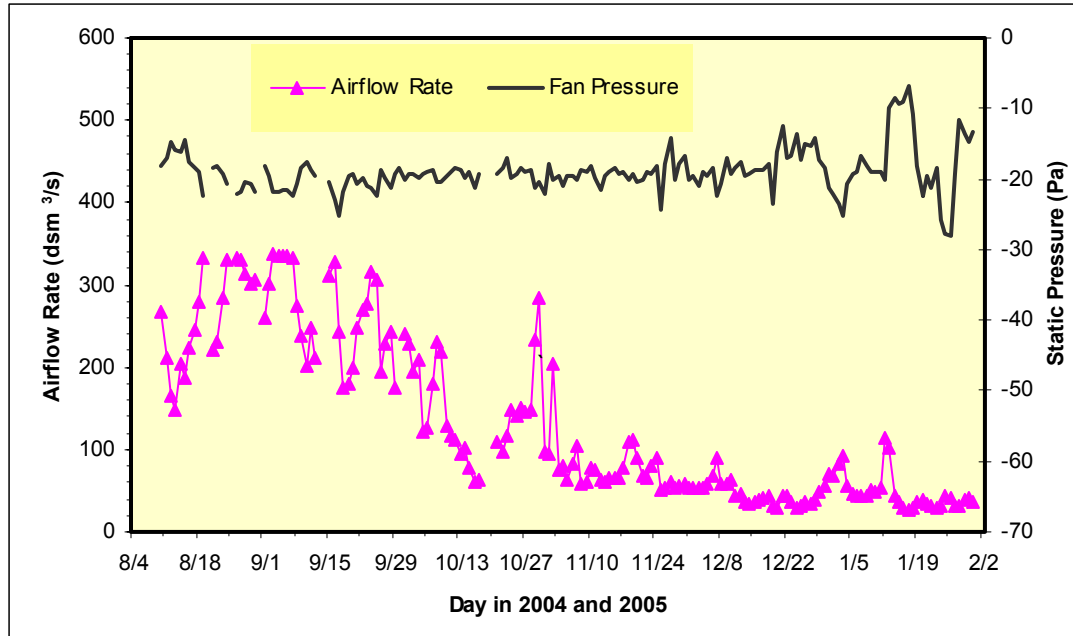


**Figure 3. Daily mean ventilation rate and barn differential pressure of the Belt-Battery barn**

The initial inventory was 167,741 hens, with the average hen weighing 1.44 kg. The hens grew to 1.7 kg in early December 2004 and lost weight to 1.63 kg by the end of the study on Jan 31, 2005. The ending inventory was 166,053 hens. The average inventory was 166,985 hens and the average hen weight was  $1.60 \pm 0.1$  kg. The total live mass ranged from 485 to 567 AU with an average of  $535 \pm 25$  AU.

### PM<sub>10</sub> Concentration and Emission

Figure 4 shows daily means of PM<sub>10</sub> concentrations and emissions from the MB barn. In August and early September, the PM<sub>10</sub> concentration decreased dramatically from a 10-d average of  $597 \pm 85$   $\mu\text{g}/\text{dsm}^3$  to a relatively stable state with an average concentration of  $239 \pm 63$   $\mu\text{g}/\text{dsm}^3$ . The overall average PM<sub>10</sub> concentration was  $265 \pm 108$   $\mu\text{g}/\text{dsm}^3$ . The initial high concentration was mainly due to new flock in the barn. New flocks are generally very active when adapting to a new environment. Such highly active flocks contribute to high PM emission and concentration. Typically it takes about six weeks for a new flock to adapt to new cage environment.

PM<sub>10</sub> concentration of the MB barn was about 45%-53% that of one HR barns reported in Lim et al. (2005), which affiliated with the same poultry company, housed similar number of hens, and had standard diet. The overall six-month average PM<sub>10</sub> concentrations of the HR barns were  $565 \pm 195$  and  $500 \pm 153$   $\mu\text{g}/\text{dsm}^3$  for the HR barn1 and 2, respectively, which agree well with the annual average PM<sub>10</sub> concentrations,  $518 \pm 74$   $\mu\text{g}/\text{dsm}^3$ , of a HR barn in Indiana (Lim et al, 2003),

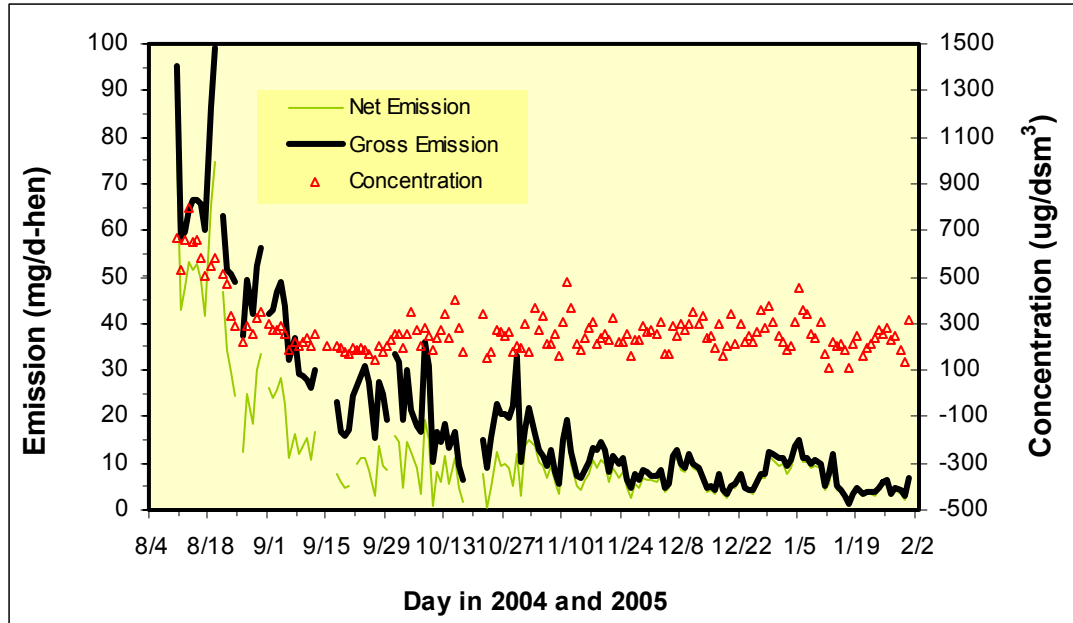


**Figure 4. Daily mean particulate matter (PM<sub>10</sub>) concentrations and emission rates of the Belt-Battery barn**

The ambient PM<sub>10</sub> concentration was used to calculate net PM<sub>10</sub> emission. Ambient PM<sub>10</sub> concentration ranged from 0 to 99% of PM<sub>10</sub> concentration at the barn exhaust fan with an average of  $31 \pm 0.2\%$ . In the first three months (hot days), the ambient PM<sub>10</sub> accounted for 47% of the exhaust concentration. In the second three months (cold days), it accounted for 18% of the exhaust concentration. Re-entrainment of exhausted particles into the poultry barn contributed to an approximately 30% increase of the PM<sub>10</sub> emission on average in the six-month period. In hot days, because of high ventilation rate and relatively small separation distance between layer barns, the re-entrainment was about 47% of PM<sub>10</sub> emission. Therefore, the gross PM<sub>10</sub> emission rates could include a significant fraction of PM<sub>10</sub> that was re-entrained into the barn.

The overall six-month average PM<sub>10</sub> emission rate was  $20 \pm 18.9$  mg/d-hen. However, the PM<sub>10</sub> emission rate was as high as 95 mg/d-hen in the beginning of the test and decreased dramatically in the first few weeks to an average of  $19.8 \pm 8$  mg/d-hen in October. As the weather got cold and barn ventilation rate decreased, the PM<sub>10</sub> emission rate fluctuated and then slowly decreased. The lowest PM<sub>10</sub> emission rate in January averaged  $7 \pm 3.6$  mg/d-hen, which was 7% of the initial PM<sub>10</sub> emission rate and 27% of PM<sub>10</sub> emission rate in late August.

The MB barns and the two HR barns (Lim et al., 2005) had very similar decreasing trends in PM<sub>10</sub> emissions as the weather got cold and ventilation rates decreased. The MB barn initially had a much higher PM<sub>10</sub> emission due to the new flock at the beginning of the study. However, the HR barns had a much higher overall PM<sub>10</sub> emission. The overall average PM<sub>10</sub> emissions were  $30 \pm 13.4$  and  $35 \pm 33$  mg/d-hen for the HR barn 1 and 2 (Lim et al. 2005) respectively. An annual average PM<sub>10</sub> emissions,  $16 \pm 3.4$  g/d-AU, which is about 51 mg/d-hen if an average of 3.2 lbs of hen weight were assumed, from an Indiana HR barn was reported by Lim et al. (2003). From this limited study, it is found that the MB barn had significantly lower PM<sub>10</sub> concentration and emission than the HR barns.

It is interesting to observe that PM<sub>10</sub> concentration in the MB barn was not affected by the decreased building ventilation rate, in contrast with PM<sub>10</sub> concentration in the HR barns which increased slowly as ventilation rates decreased and the weather cooled down. However, because emission rate is a product of ventilation rate and concentration, PM<sub>10</sub> emission rates of layer barns were strongly affected by ventilation rate. Thus, PM<sub>10</sub> emission rates of the layer barns decreased as the ambient temperature decreased.

### TSP Concentration and Emission

Figure 5 shows mean TSP concentrations and emission rates from the MB barn 1. At the exhaust of the MB barn, TSP concentration increased as ventilation rate decreased due to lower outdoor temperature. The concentration fluctuated day by day, but overall increased from 1767 to 4247  $\mu\text{g}/\text{dsm}^3$  with a six-month average of  $3070 \pm 675 \mu\text{g}/\text{dsm}^3$ . The HR barn and MB barn had TSP concentrations very similar to the HR barn 1, which had an average TSP concentration of  $2,795 \pm 745 \mu\text{g}/\text{dsm}^3$  (Lim et al., 2005). Annual average TSP concentration of an Indiana layer barn was  $1887 \pm 563 \mu\text{g}/\text{dsm}^3$  (Lim et al. 2003), which is lower than that of the Ohio layer barns. Indoor environment, management practices, building ventilation, diet, and hen activity will likely affect PM emission and concentrations.

The TSP emission decreased dramatically in September and October and then reached a relatively stable state in the colder months. The average TSP emission rates were  $272 \pm 96 \text{ mg}/\text{d-hen}$  in September and October and  $93 \pm 24 \text{ mg}/\text{d-hen}$  in the colder months. Both the HR barn and the MB barn barns had decreasing trends in TSP emission as outdoor temperature decreased. However, TSP emission in the MB barn had a high initial value of  $500 \text{ mg}/\text{d-hen}$  and a relative steep decrease while the HR barn had an initial high value of  $359 \mu\text{g}/\text{dsm}^3$  and a relatively slow decrease. It is very likely that the new flock contributed to the high initial TSP concentration and emission. Ventilation rates were also strongly associated with TSP emission in the layer barns. In cold months (Nov., Jan. and Feb.), TSP emissions were stable for both types of barns with an average TSP emission of  $93 \pm 24$  and  $103 \pm 31 \text{ mg}/\text{d-hen}$  from the MB barn and the HR barn, respectively. The overall mean TSP emission was  $168 \pm 110$  and  $146 \pm 96.6 \text{ mg}/\text{d-hen}$  from the MB barn and the HR barn, respectively. Statistical analysis of variance showed that TSP emissions from the two types of barns in cold months were not statistically different ( $P=0.4485$ ). A paired t-test showed that TSP emissions in the warm months also showed no statistical difference ( $P=0.395$ ). The annual average TSP emission from the Indiana layer barn was  $63 \pm 15 \text{ g}/\text{d-AU}$  (Lim et al. 2003), which is about  $201 \text{ mg}/\text{d-hen}$  and higher than that of the Ohio layer barns.

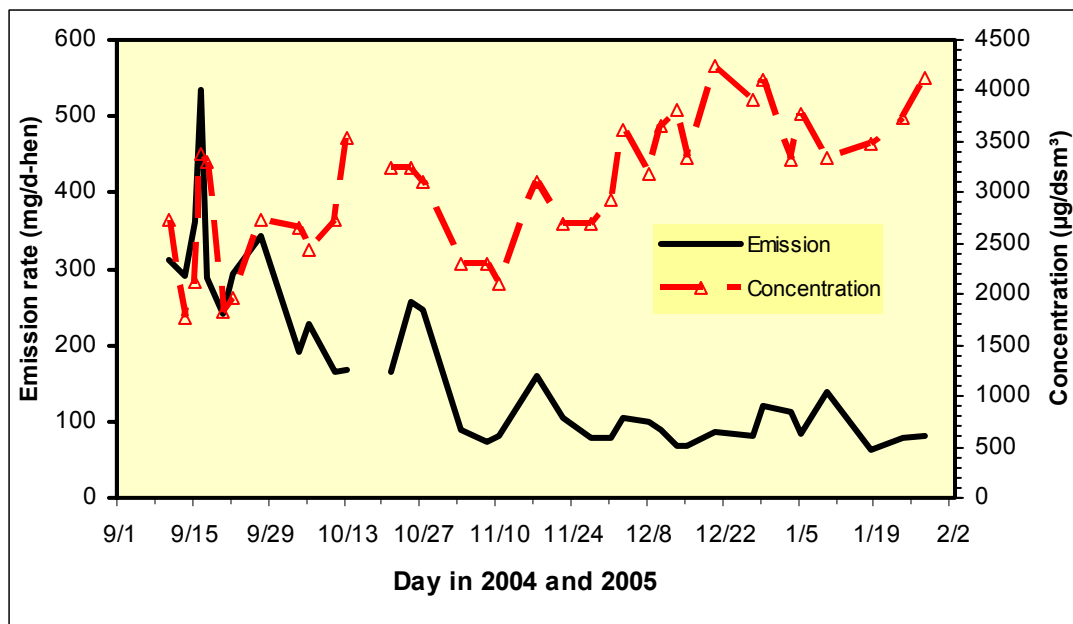


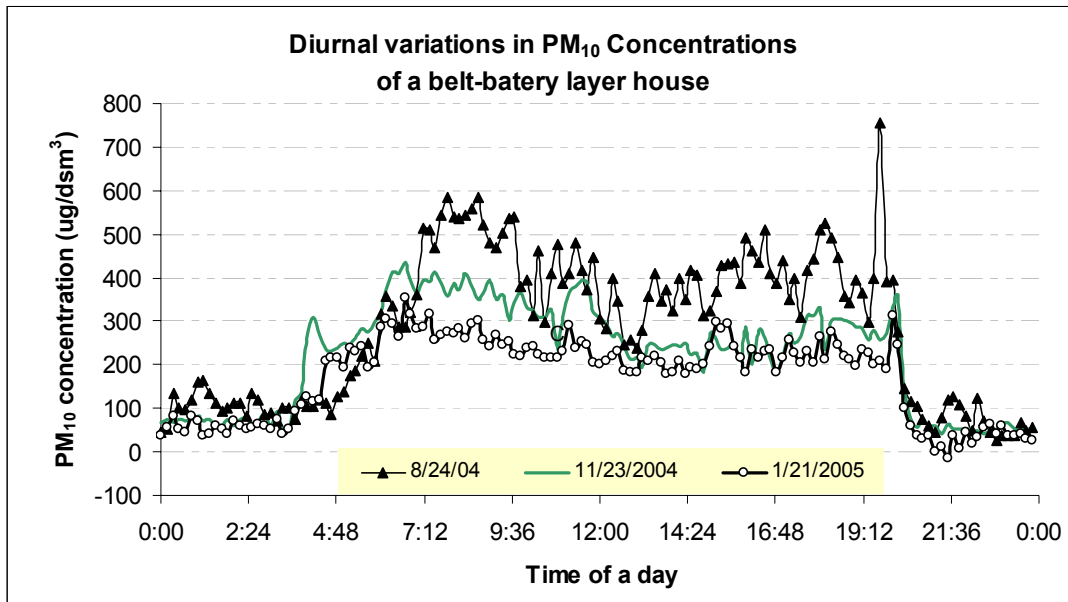
**Figure 5. Mean total suspended particles (TSP) concentrations and emissions**

The ratios of  $\text{PM}_{10}$  to TSP were 5-16% with an average of  $9 \pm 3\%$  in the MB barn and 14-41% with an average of  $25 \pm 5\%$  in the HR barn.

According to the emission rates, it would take about 4.1 million hens in the MB barn or 4.7 million hens in the HR barn to emit 250 tons of TSP per year, which is the emission threshold regulated by the CAA Prevention of Significant Deterioration (PSD) permit program. It would take about 13.7 million hens in the MB barn or 8.5 million hens in the HR barns to emit 100 tons of  $\text{PM}_{10}$  per year, which is the emission threshold regulated by the CAA Title V permit.

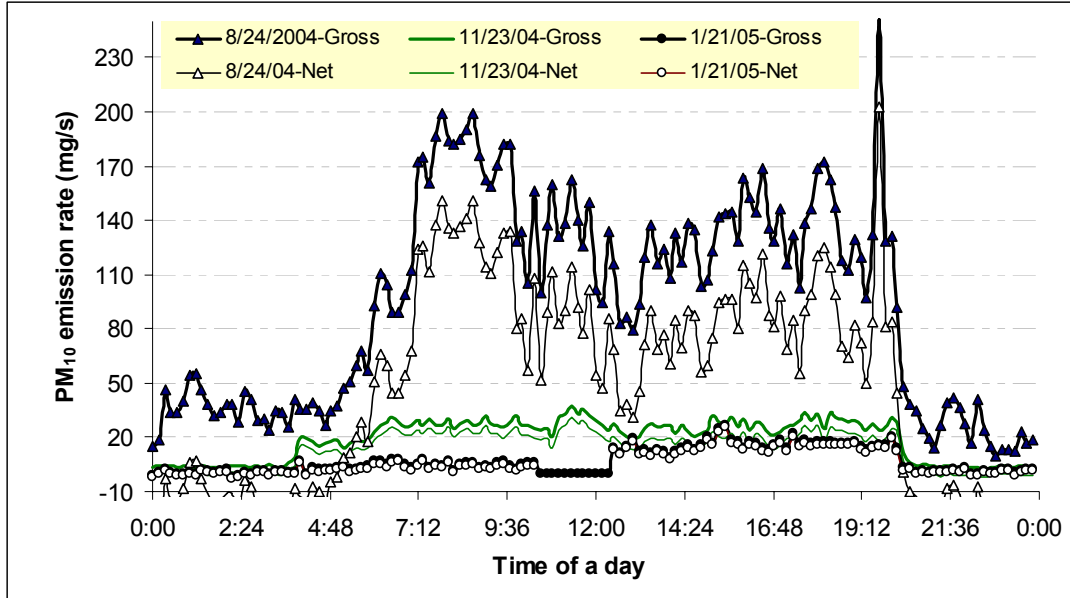
### Diurnal Variations in PM<sub>10</sub> Concentrations and Emission Rates

Figure 6 shows daily variations in PM<sub>10</sub> mass concentrations at an exhaust of the MB layer barn. The continuous measurement results clearly indicated effects of light control on indoor PM<sub>10</sub> concentrations. Each day at 4:00 a.m. when the lights were turned on, PM<sub>10</sub> concentrations increased significantly. Each day when the lights were turned off at 8:00 p.m., the indoor PM<sub>10</sub> concentrations significantly dropped. At the end of the day, before the lights were turned off, dust concentration reached its daily peak. These results agree with previous studies (Carpenter, 1986; Maghirang et al., 1991). Statistical analysis shows that dust concentrations during light hours were statistically different from those during dark hours ( $P < 0.05$ ).



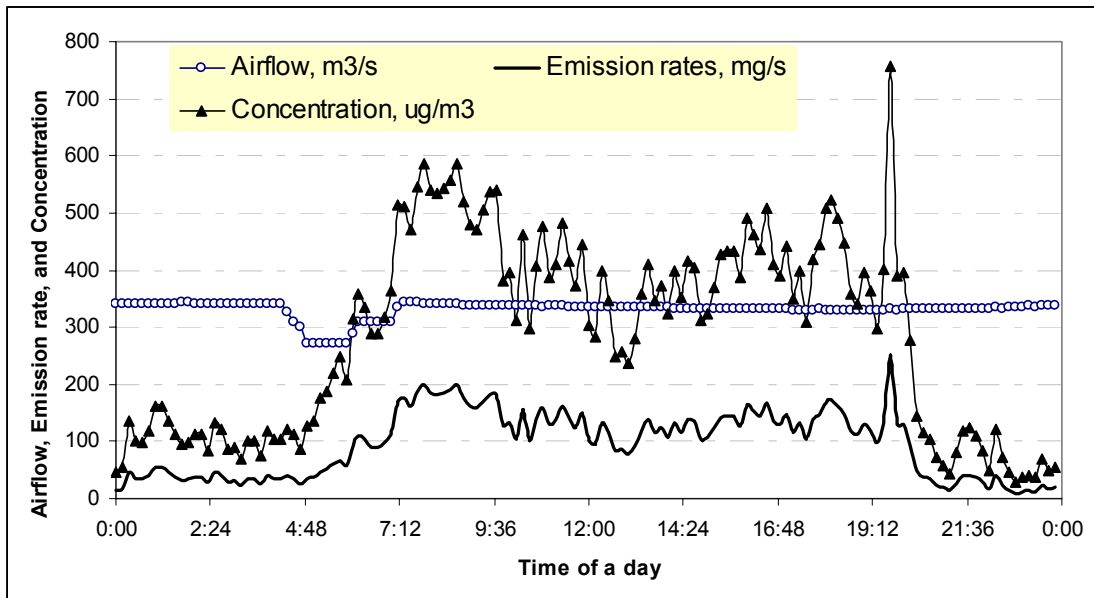
**Figure 6. Diurnal variations in PM<sub>10</sub> concentrations at an exhaust fan of the manure belt-battery layer house**

Figure 7 shows daily variations in PM<sub>10</sub> emission rates of the MB layer barn. The 10-minute average emission rates within 24-hour periods show strong effects of light control on PM<sub>10</sub> emission rates in August and weaker effects in November. There is no clear diurnal pattern in January due to minimum ventilation. PM<sub>10</sub> emission rates increased significantly when the lights were turned on at 4:00 am and dropped significantly as the lights were turned off at 8:00 pm in August. In January, when minimum ventilation was in operation, there was no clear diurnal trend in PM<sub>10</sub> emission rates. The diurnal emission rate patterns agree with the concentration diurnal patterns very well on the day in August, but not on the January day. Statistical analysis shows that dust PM<sub>10</sub> emission rates during light hours were statistically different from rates during dark hours on the days in August and November ( $P < 0.05$ ), but not on the day in January.



**Figure 7. Diurnal variations in PM10 emission rates of a manure belt-battery layer house**

Figure 8 shows an example of daily variations in barn airflow, PM<sub>10</sub> concentrations, and PM<sub>10</sub> emission rates. It confirms the dominant light control effects on PM<sub>10</sub> indoor concentration and emission rates.



**Figure 8. Example daily variations in barn airflow, PM10 concentrations, and PM10 emission rates**

### Conclusions

The overall average PM<sub>10</sub> concentration of the MB barn was 265±108 µg/dsm<sup>3</sup>. The overall average PM<sub>10</sub> emissions were 20±18.9 mg/d-hen.

The TSP concentration of the MB barn fluctuated day by day, but overall increased from 1643 to 4025 µg/dsm<sup>3</sup> with a six-month average of 3070±675 µg/dsm<sup>3</sup>.

TSP emissions of both MB and HR barns decreased as outdoor temperature decreased. However, in cold months, TSP emissions were stable for both types of barns, with average TSP emission rates of  $93\pm 24$  and  $103\pm 31$  mg/d-hen from the MB barn and the HR barn, respectively. The overall mean TSP emission rates were  $168\pm 110$  and  $146\pm 97$  mg/d-hen from the MB barn and HR barn 1, respectively. Statistical analysis of variance showed that TSP emissions from the two barns in cold months were not statistically different ( $P=0.4485>0.05$ ). A paired t-test showed that TSP emissions in the warm months were not statistically different either ( $P=0.395$ ).

According to the emission rates, it would take about 4.1 million hens in the MB barn or 4.7 million hens in the HR barn to emit 250 tons of TSP per year. It would take about 13.7 million hens in the MB barn or 8.5 million hens in the HR barns to emit 100 tons of  $PM_{10}$  per year.

New hen flock contributed to higher TSP and  $PM_{10}$  concentrations and emissions from the MB barn. High ventilation rates were also strongly associated with high  $PM_{10}$  and TSP emissions in the layer barns.

During high ventilation rate periods, there are strong diurnal patterns of  $PM_{10}$  concentrations and emission rates associated with the light control schedule.  $PM_{10}$  concentrations and emission rates during light hours of high ventilation rate periods are significantly higher ( $P<0.05$ ) than during dark hours of high ventilation rate periods. There is no clear diurnal pattern in  $PM_{10}$  concentrations and emission rates during minimum ventilation periods.

### References

- Carpenter, G.A. 1998. Dust in livestock buildings – review of some aspects. *J. Agric. Eng. Res.* 33:227-241.
- EPA. 2005. The U.S. EPA air compliance consent agreement with animal feeding operations. <http://www.epa.gov/compliance/resources/agreements/caa/cafo-agr-050121.pdf>. Last accessed July 28, 2005.
- Heber, A.J., T.-T. Lim; J.Z. Gallien; J.-Q. Ni; P.C. Tao, A.M. Millmier, L.D. Jacobson, J.A. Koziel, S.J. Hoff, Y. Zhang, and G.B. Baughman. 2002. Quality assured measurements of animal building emissions: Part 2. Particulate matter concentrations. *Symposium on Air Quality Measurement Methods and Technology*, San Francisco, CA. Nov. 13-25, Air and Waste Management Assoc.: Pittsburgh, PA.
- Heber, A.J. 2004. Measurement and control of ammonia, dust and odor emissions from layer houses. *Multi-State Poultry Meeting*, Indianapolis, IN, May 25-27
- Heber, A.J., T.T. Lim, J.-Q. Ni, P.-C. Tao, A.M. Schmidt, J.A. Koziel, S.A. Hoff, L.D. Jacobson, Y. Zhang, and G.B. Baughman. 2005. Quality assured measurements of animal building emissions: Part 2. Particulate matter concentrations. *Journal of Air and Waste Management*, accepted pending revision.
- Jerez, S., Y. Zhang, J. McClure, L.D. Jacobson, A.J. Heber, J. Koziel, S.J. Hoff, and D.B. Beasley. (*in press*). Comparison of total particulate emission using tapered element oscillating microbalance and a TSP sampler. *AWMA Journal*.
- Liang, Y., H. Xin, E.G. Wheeler, R.S. Gates, H. Li, J.S. Zajackowski, P. Topper, K.D. Casey and F.J. Zajackowski. 2004. Ammonia emission for US poultry houses: layer hens. ASAE Paper No. 044104. St. Joseph, Mich.: ASAE.
- Lim, T.-T., A.J. Heber, J.-Q. Ni, J.Z. Gallien, and H. Xin. 2003. Air quality measurements at a laying hen house: particulate matter concentrations and emissions. *Air Pollution from Agricultural Operations*, Durham, NC, USA, October 12-15., p.249-256.
- Lim, T.T., H. Sun, J.-Q. Ni, L. Y. Zhao, C. Diehl, A.J. Heber, and P.C. Tao. 2005. Effect of flow-through particulate impaction curtain on PM emissions from a high-rise layer barn. ASAE paper 054013. St. Joseph, Mich.: ASAE.
- Maghirang, R.G., H.B. Manbeck, W.B. Roush, and F.V. Muir. 1991. Air contaminant distributions in a commercial laying house. *Trans. ASAE* 34: 2171-2180.

Ni, J.-Q, A.J. Heber, H. Sun, S.M. Hanni, C. Diehl, T.T. Lim, L.Y. Zhao, and M. Darr. 2005. Application of vibration sensors for fan monitoring to improve measurement quality at a large layer barn. ASAE paper 054013. St. Joseph, Mich.: ASAE.

Ji-Qin Ni<sup>1</sup>, Technical Director; Albert J. Heber<sup>1</sup>, Professor; Hua-Wei Sun<sup>2</sup>, Research Associate; Sam M. Hanni<sup>1</sup>, Research Assistant; Claude A. Diehl<sup>1</sup>, Research Engineer; Teng T. Lim<sup>1</sup>, Research Scientist; Lingying Zhao<sup>2</sup>, Assistant Professor; Matt Darr<sup>2</sup>, Research Associate

NRC. 2003. *Air emissions from animal feeding operations: current knowledge, future needs*. Washington, DC: The National Research Council of the National Academies, The National Academies Press.

Sun, H, T.T. Lim, J.-Q. Ni, A.J. Heber, L.Y. Zhao, C.A. Diehl, P.C. Tao, and S. Hanni. 2005. Ammonia emissions from a belt-battery layer house. ASAE paper 054166. St. Joseph, Mich.: ASAE.

Takai, H., S. Pedersen, J.O. Johnsen, J.H.M. Metz, P.W.G.G. Koerkamp, G.H. Uenk, V.R. Phillips, M.R. Holden, R.W. Sneath, J.L. Short, R.P. White, J. Hartung, J. Seedorf, M. Schroder, K.H. Linkert, and C.M. Wathes. 1998. Concentrations and emissions of airborne dust in livestock buildings in Northern Europe. *J. Agri. Engng Res.* 70(1): 59-77.

Xin, H. 2005. Ammonia emissions & potential mitigation options for U.S. poultry facilities. Presentation at the North Atlantic Poultry Health and Management Conference, May 10. <http://www.abe.iastate.edu/Xin/Atlantic-talk-5-10-2005-Xin.pdf>.

Wang, X., Y. Zhang, L. Y. Zhao, and G. L. Riskowski. 1999. Development of a multi-point aerosol sampler using critical flow control devices. *Transactions of ASHRAE* 105(2): SE-99-17-03.



## Optimization of Air Sampling Strategies for Monitoring Ammonia Emissions from Poultry Layer Facilities

Lingying Zhao<sup>1</sup>, Albert J. Heber<sup>2</sup>, Teng T. Lim<sup>2</sup>, J.-Q. Ni<sup>2</sup>, and P.C. Tao<sup>2</sup>

<sup>1</sup>Ohio State University, Columbus, OH 43210, USA

<sup>2</sup>Purdue University, West Lafayette, IN 49707, USA

### Abstract

Ammonia from concentrated poultry layer houses result in significant environmental and health concerns. The emission data are highly needed by government agency, producers, and researchers to regulate and mitigate the emissions from poultry facilities. Since the complex spatial and temporal variations of the ammonia emission problem due to many affecting factors, accurately estimating and monitoring ammonia emissions from poultry laying houses have been challenging. The Purdue mobile lab method for air emission measurement, which continuously monitoring air emissions from poultry facilities, can provide relatively complete and accurate ammonia emission information, but it involves high cost and long monitoring time. Sufficient air sampling rates for monitoring ammonia emissions are needed information for wide application of this methodology and other air monitoring methodologies. This study analyzed ammonia emission data of several 6-month continuous, intensive measurements of large egg laying houses using the Purdue method with two sets of ammonia gas analyzers, that one switched between nine exhaust locations and the other kept at one location. Analysis of variance was used to evaluate spatial and temporal variations of ammonia emissions. Factors associated with spatial and temporal variation of air emissions were evaluated with sensitivity analysis. The study results showed that spatial variation of ammonia emission in a conventional high-rise layer facility is relatively small. Air sampling periods should be at least two weeks for each major seasonal weather condition. The optimum length of time for determining semi-annual emission factors is six weeks, such as two weeks in January, March, and May, respectively.



## Predicting NH<sub>3</sub> Emissions from Manure N for Livestock Facilities and Storages: A Modified Mass Balance Approach.

H. M. Keener<sup>1</sup> and L. Zhao

### Abstract

NH<sub>3</sub> levels and resulting emissions during the handling of manure at animal-production facilities have significant health, safety, odor-generation, and environmental impacts. In addition, NH<sub>3</sub> levels are impacting the profitability and growth of the livestock industry and forcing adoption of new technology. Determining NH<sub>3</sub> emissions is costly using the current approach of measuring ammonia concentrations and airflow from a facility. This paper looks at using N-balances to determine the upper limit on NH<sub>3</sub>-N emissions for both forced and naturally ventilated livestock facilities. The analysis uses a controlled volume approach for inputs and outputs from the system and N/ash ratios. Considered in the analysis are body growth, milk and egg production, mortality and leachate as materials leaving the system. However, this method does not distinguished for losses of N as N<sub>2</sub> or NO<sub>x</sub>'s. Although the method can not predict daily cycles in emissions or maximum concentrations, it can provide an accurate estimate of the maximum theoretical levels for NH<sub>3</sub>-N emissions over long production cycles (several days to months) if sampling gives good precision. As such, results are to be interpreted as daily, weekly or yearly averages. It does not require measuring total masses of materials into and from the system, but is dependent on obtaining adequate, representative samples of feed and manure at entry/exit points of the housing and storage systems. Generalized equations for predicting emissions from all classes of livestock operations are presented. Research using this N-balance method was simple, low cost, and accurate (based on results and reported literature values) in predicting upper limits on NH<sub>3</sub> emissions in the air leaving a 1.6 million caged layer poultry facility using two types of manure management: belt/composting and deep pit. Specific results based on the study showed clear advantages of belt/composting over conventional deep-pit systems, with total emissions less than half that of the conventional caged layer systems.

Keywords: ammonia, emissions, livestock environment, poultry manure, nitrogen balance, odor.

### Background

During the past decade, emissions from concentrated feeding livestock facilities have become a significant environmental issue as it relates to odors and greenhouse gases, in particular NH<sub>3</sub>. Already, in Western Europe, legislation is in place to require the reduction of NH<sub>3</sub> emissions by up to 50% (Groot Koerkamp, 1994). This issue is a major constraint to the profitability and growth of livestock industries and mandate new approaches to livestock housing and manure management. Evaluating the effects of these new methods on emissions from livestock buildings for full scale operations can be quite expensive and labor intensive using current methodologies of continuous monitoring of airflows and emission levels (Heber et al., 2001; NRC 2003).

The goal of this study was to develop the theory for a modified mass balance approach to predicting NH<sub>3</sub>-N emissions for livestock operations and apply this method to a 1.6 million bird poultry facility in Ohio using two types of manure management: belt/composting and deep pit.

### Theory

N balances for animal production system enable predicting upper limits on ammonia emissions. Figure 1 is a schematic of an animal production system showing inputs and outputs, generalized for the case of body growth, milk and egg production. It also includes mortality and leachate as materials leaving the system. Analysis of this production system for NH<sub>3</sub>-N assumes no other gaseous losses of N.

---

<sup>1</sup>The authors are Harold M. Keener, professor, and Lingying Zhao, assistant professor, Department of Food, Agricultural, and Biological Engineering, Ohio Agricultural Research and Development Center, Ohio State University. Corresponding author: Harold M. Keener. e-mail: keener.3@osu.edu.

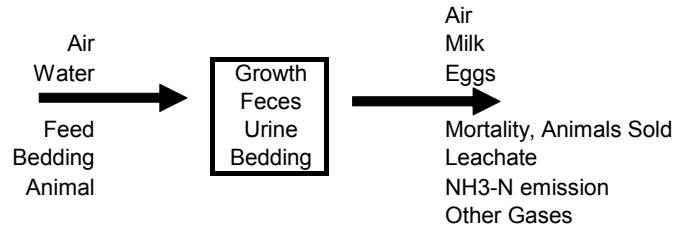


**Figure 1. Flow diagram of animal production system showing inputs, storage and output variables.**

To simplified the presentation of equations used in the analysis the notations presented in Table 1 were adopted. The nitrogen balance for the system based on ( $N_{\text{storage}} = N_{\text{in}} - N_{\text{out}}$ ) is given by

$$\sum_{i=6}^9 x_{N_i} \frac{dm_i}{d\theta} \cong \sum_{i=1}^5 x_{N_i} m_i' - \sum_{i=10}^{14} x_{N_i} m_i' - N_{15} \quad (1)$$

For an ash balance on the system the equation is

$$\sum_{i=6}^9 x_{A_i} \frac{dm_i}{d\theta} = \sum_{i=1}^5 x_{A_i} m_i' - \sum_{i=10}^{14} x_{A_i} m_i' \quad (2)$$

**Table 1. Variables and nomenclature used in mass balance equations for prediction NH<sub>3</sub>-N emissions from livestock facilities.**

<u>Variables</u>	<u>Subscript</u>
$\theta$ = time, day	$i =$
$m_i$ = mass of $i$ , kg	6, growth of animals in system
$m_i'$ = mass flow rate, kg/day	7, feces in system
$dm_i/d\theta$ = rate of change, kg/day	8, urine in system
$x_{N_i}$ = nitrogen content, dec	9, bedding in system
$x_{A_i}$ = ash content, dec.	10, air out of system
$R_i = x_{N_i}/x_{A_i}$ , nitrogen to ash ratio, dec	11, milk out of system
$N_i$ = total nitrogen in $i$ , kg/day	12, eggs out of system
<u>Subscript</u>	13, mortality, animals sold out of system
$i = \dots\dots$	....14, leachate
1, air in	....15, NH <sub>3</sub> -N emission
2, water in	A, ash
3, feed in	N, nitrogen
4, bedding in	M, manure
5, animals in	

Solving equation 1 for  $N_{15}$  (the nitrogen emitted as NH<sub>3</sub>-N gives

$$\begin{aligned} N_{15} &\leq \sum_{i=1}^5 x_{N_i} m_i' - \sum_{i=6}^9 x_{N_i} \frac{dm_i}{d\theta} - \sum_{i=10}^{14} x_{N_i} m_i' \\ &= \sum_{i=3}^5 x_{N_i} m_i' - x_{N_6} \frac{dm_6}{d\theta} - \sum_{i=7}^9 x_{N_i} \frac{dm_i}{d\theta} - \sum_{i=11}^{14} x_{N_i} m_i' \end{aligned} \quad (3)$$

The final form of (3) assumes N in the air entering the system passes through the system and no N is in the water entering the system. The term  $\sum_{i=7}^9 x_{N_i} \frac{dm_i}{d\theta}$  is the total nitrogen in the manure.

Using equation 2, the total ash in the manure is given by

$$\sum_{i=7}^9 x_{A_i} \frac{dm_i}{d\theta} = \sum_{i=3}^5 x_{A_i} m_i' - x_{A_6} \frac{dm_6}{d\theta} - \sum_{i=11}^{14} x_{A_i} m_i' \quad (4)$$

Now from sampling the manure and laboratory analysis the manure N/A ratio,  $R_M$ , can be evaluate. But it is also true that

$$R_M = \sum_{i=7}^9 x_{N_i} \frac{dm_i}{d\theta} / \sum_{i=7}^9 x_{A_i} \frac{dm_i}{d\theta} \quad (5)$$

Substituting (5) and (4) into (3) gives

$$N_{15} \leq \sum_{i=3}^5 x_{N_i} m_i' - x_{N_6} \frac{dm_6}{d\theta} - \sum_{i=11}^{14} x_{N_i} m_i' - R_m \left[ \sum_{i=3}^5 x_{A_i} m_i' - x_{A_6} \frac{dm_6}{d\theta} - \sum_{i=11}^{14} x_{A_i} m_i' \right] \quad (6)$$

The advantage of (6) over (1) for doing N mass balance and estimating  $\text{NH}_3\text{-N}$  losses is no weighting of the manure is required. A second advantage of (6) compared to the conventional method of continuous sampling of airflow rates and  $\text{NH}_3\text{-N}$  concentration for exhausting air is avoidance of the high equipment cost, maintenance and labor to operate continuous monitoring equipment. However, this method does not distinguished for losses of N as  $\text{N}_2$  or  $\text{NO}_x$ 's. Also, it would not predict daily cycles in emissions or maximum concentrations. It can however, provide an accurate estimate of the maximum theoretical levels for  $\text{NH}_3\text{-N}$  emissions over long production cycles (several days to months) if sampling gives good precision. As such, results are to be interpreted as daily, weekly or yearly averages.

Eq 6 can be used to predict the upper limit on  $\text{NH}_3\text{-N}$  emissions for open and/or naturally ventilated building. Such structures do not lend themselves to the more common method of measuring airflows and  $\text{NH}_3$  concentrations leaving a building. For example, for a concrete free stall dairy barn with lactating cows, terms containing 5, 6, 12, 13, and 14 would probably be zero. For a deep pit swine finishing house, the terms containing 4, 5, 9, 11, 12, and 14 would probably be zero. Data for the non-zero terms would be based on time periods conducive to accurate sampling.

Keener et al., (2002) used eq. 6 for analysis of two types of caged layer facilities. Information from that paper are presented here to illustrate how the method can be applied. In that study, results using the modified mass balance approach were compared with measured emissions based on airflows and exhaust  $\text{NH}_3\text{-N}$  concentrations and with published literature. For analysis purposes, it was assumed the terms  $\frac{dm_6}{d\theta}$ ,  $m_4'$ ,  $m_5'$ ,  $m_{11}'$ ,  $m_{13}'$  and  $m_{14}'$  were  $\cong$  zero. Because the birds were mature, the assumption on  $\frac{dm_6}{d\theta}$  (i.e. changes in their body composition, storage or release of ash and nitrogen) could be justified.

Also, no bedding was used, no animals were placed, no milk was produced, mortality was very low, and no leachate was observed during the analysis periods. The equation to evaluate  $N_{15}$  becomes

$$N_{15} \leq x_{N_3} m_3' - x_{N_{12}} m_{12}' - R_m \left[ x_{A_3} m_3' - x_{A_{12}} m_{12}' \right] \quad (6b)$$

For yearly emissions per bird, eq. 6b becomes

$$EM_{\text{NH}_3\text{-N}} = 365 N_{15}/n_b \quad (\text{kg NH}_3\text{-N bird}^{-1} \text{ yr}^{-1}), \quad (7)$$

where  $n_b$  was the number of birds in the building.

### Experimental Facilities

The Mad River facility of the Daylay Egg Farm, located near West Mansfield, Ohio, is a modern, 1.6 million bird, caged layer facility for the production of chicken eggs (fig. 2). The birds are housed in a total of eight buildings. Four buildings are of the deep-pit design and house 150,000 birds each. Manure is removed yearly from these buildings and directly land applied. The other four buildings were built in a 1997 expansion and house 250,000 birds each. They incorporate a belt conveyor system for manure

removal. Manure on the belt is delivered to two separate buildings (12 lanes and 6 lanes, respectively) where it is composted, using Salmeter composters, into a dry product suitable for fertilizer applications.

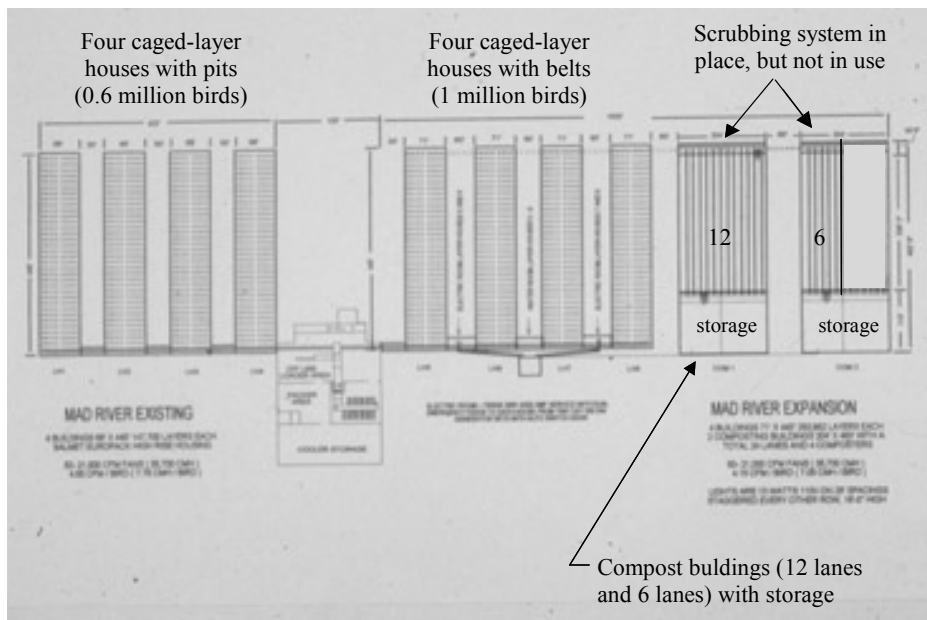


**Figure 2. Schematic of the Daylay Mad River facility (Keener, et al., 2002).**

All of the buildings have significant ventilation. The deep-pit caged layer houses each have 36 side-mounted hooded fans (18 per side) located in the pit area, which draw air down across the birds (maximum rate  $0.13 \text{ m}^3 \text{ min}^{-1} \text{ bird}^{-1}$ ,  $4.7 \text{ cfm bird}^{-1}$ ) and out. The new layer buildings are vented through the roof using a bank of nine large computer-controlled fans on each house ( $0.119 \text{ m}^3 \text{ min}^{-1} \text{ bird}^{-1}$ ,  $4.2 \text{ cfm bird}^{-1}$ ). Inlets are located along the entire sidewall length. The composting buildings are vented at one end using eight fans on one building and four fans on the other, each with a capacity of  $566 \text{ m}^3 \text{ min}^{-1}$  ( $20,000 \text{ cfm}$ ).

### Experimental Procedure

Sampling data on ammonia measurements were made on 22-23 March and 17-18 July 2000 in cooperation with the Wisconsin Department of Natural Resources (Keener, et al., 2002). Instantaneous ammonia concentration measurements were made from deep-pit caged layer houses 1 and 4 at the exit of the hooded exhaust fans using colorimetric stain tubes with ranges of 0.25 to 3 ppm, 2 to 30 ppm, or 5 to 70 ppm,  $\pm 15\%$  error (National Dräger Inc., Pittsburgh, Pa.). These measurements were also made for belt caged layer house 8 at the entrance to the exhaust fans and for the two compost buildings at the exit from the shuttered fans. Airflows from fans were based on rated capacity and no verification of accuracy was attempted, as random operation of fans was a much greater source of error. Results from calculations using airflows were used only as a gauge of the range for  $\text{NH}_3$  emissions and not a prediction of absolute amounts lost.

On day 2 of each test, manure and compost samples were collected. Eight manure samples were collected from the four deep-pit caged layer houses, two from each house. Each sample was a composite of grab samples from the top or the middle of the manure windrows at four or five different locations. For the four caged layer houses using manure belts, five manure samples were collected randomly over a 30-minute interval from the cross conveyor belt transferring manure to the compost building. For the compost buildings, five samples of finished compost were collected, one each from lanes 2, 6, and 10 in building 1 and from lanes 2 and 4 in building 2. All samples were sent to the OARDC/OSU analytical laboratory for analysis of pH, solids, ash, total carbon, inorganic carbon,  $\text{NH}_3\text{-N}$ ,  $\text{NO}_3\text{-N}$ , and total N. The feed was analyzed for moisture, ash, and nitrogen. Values used for egg composition were estimated from general literature. Solution of the mass balance made use of the fact that feeding rate was known on a per bird basis and that ash per bird could be defined at all points in the system.

## Results

Table 2 gives daily feed rate, daily egg production rate along with chemical composition of feed, eggs, deep-pit manure (buildings 1-4), belt manure (buildings 5-8) and compost (compost buildings). The deep-pit manure had an N/ash content of 0.06072 and 0.09143 for March and July, respectively. Belt manure was 1 to 3 days old and had an N/ash content of 0.18705 in March and 0.19096 in July. The compost had a N/ash content of 0.16729 for March and 0.16373 for July.

**Table 2. Mean ( $\mu$ ) and standard deviation (sd) of feed rate, production level and chemical analysis of feed, egg, manures, and compost used in nitrogen balances for Daylay facilities on 22 March and 18 July 2000 (Keener et al., 2002)**

Description		per Bird kg/day	DM (%)	Ash (%)	TC (%)	IC (%)	N (%)	NH <sub>3</sub> -N ( $\mu\text{g g}^{-1}$ )	NO <sub>3</sub> -N ( $\mu\text{g g}^{-1}$ )	Rm N/ash
Feed input	$\mu$	0.09091	89.60	13.73			2.82			
	sd	0.00455	0.15	0.65			0.31			
Eggs	--	0.05227	34.10	10.00			2.05			
22 March 2000										
Deep-pit manure (buildings 1-4)	$\mu$		40.20	48.42	26.91	3.39	2.94	19038	81.1	0.06072
	sd		10.05	9.09	3.83	0.67	0.81	11295	23.9	
Belt manure (buildings 5-8)	$\mu$		46.99	30.26	33.37	1.94	5.66	6810.9	232.4	0.18705
	sd		6.65	1.96	1.06	0.31	0.99	2631.4	57.3	
Compost buildings	$\mu$		82.02	37.18	31.11	2.14	6.22	8150.2	256.1	0.16729
	sd		0.97	1.80	1.07	0.23	0.24	763.3	38.7	
18 July 2000										
Deep-pit manure (buildings 1-4)	$\mu$		70.81	43.97	28.96	2.78	4.02	4782.9	93.8	0.09143
	sd		12.19	5.08	1.76	0.44	0.77	1551.6	14.1	
Belt manure (buildings 5-8)	$\mu$		51.71	30.74	33.85	1.68	5.87	6566.3	211.9	0.19096
	sd		8.07	3.41	2.25	0.38	0.48	2578.1	24.7	
Compost buildings	$\mu$		90.20	34.08	32.28	1.92	5.58	4846.6	213.1	0.016373
	sd		0.91	1.32	1.11	0.14	0.57	1245.4	37.4	

Table 3 summarizes the nitrogen balances for two caged layer manure management systems based on N fed to the animal, N in the eggs produced, and N emitted by using equation 7. Results showed that the average N retained for the March and July studies was 0.556 kg bird<sup>-1</sup> yr<sup>-1</sup> and 0.209 kg bird<sup>-1</sup> yr<sup>-1</sup> for the belt/compost system compost and conventional deep-pit manure, respectively. This represented 81% and 30% of N excreted by the birds, respectively.

Table 3 also lists the nitrogen emissions results for March and July. Total nitrogen emission during March for a conventional caged layer deep-pit system (DP) was 0.477 kg (1.05 lb) N bird<sup>-1</sup> yr<sup>-1</sup>. This would be 0.631 kg NH<sub>3</sub> bird<sup>-1</sup> yr<sup>-1</sup> and is very similar to the value that Battye et al. (1994) reported of 0.598 kg NH<sub>3</sub> bird<sup>-1</sup> yr<sup>-1</sup> for laying hens >6 months of age. Total nitrogen emission during March, based on compost N level, for the belt/compost caged layer system (CLB-CB) was calculated to be 0.129 kg (0.284 lb) N bird<sup>-1</sup> yr<sup>-1</sup>. This would be 0.166 kg NH<sub>3</sub> bird<sup>-1</sup> yr<sup>-1</sup> and is 25% of the value for the deep-pit system. For the DP and CLB-CB systems, the calculated NH<sub>3</sub>-N loss using estimated airflow rates and measured ammonia concentrations in the exhaust air were 0.550 and 0.437 kg (1.213 and 0.963 lb) N bird<sup>-1</sup> yr<sup>-1</sup>, respectively. Losses of NH<sub>3</sub> only from the layer building for the CLB-CB system, using a mass balance approach, were estimated at 0.057 kg bird<sup>-1</sup> yr<sup>-1</sup>, compared to 0.034 kg bird<sup>-1</sup> yr<sup>-1</sup> cited by Groot Koerkamp (1994). Results in March using airflows and NH<sub>3</sub> concentrations were very approximate because airflows were varying during the data collection period. For the conventional deep-pit caged layer system, the exhaust streams measured 5 to 60 ppm NH<sub>3</sub> v/v when all exhaust fans (32 per building) were running, while the belt caged layer system had 5 to 10 ppm NH<sub>3</sub> v/v (Keener et al., 2002).

**Table 3. Nitrogen balance (kg bird<sup>-1</sup> yr<sup>-1</sup>) for Daylay operation, March and July 2000.**

System <sup>[a]</sup>	Measured Variable	Feed N	Egg N	N manure DP or CB	Total NH <sub>3</sub> -N loss	NH <sub>3</sub> -N loss CLB	NH <sub>3</sub> -N loss CB
<b>March</b>							
DP	Manure Ash & N	0.823	0.133	0.213 <sup>b</sup>	0.477		
DP	NH <sub>3</sub> loss	0.823	0.133		0.550		
CLB-CB	Manure & Compost Ash & N	0.823	0.133	0.561 <sup>b</sup>	0.129	0.057	0.072 <sup>d</sup>
CLB-CB	NH <sub>3</sub> loss	0.823	0.133		0.437 <sup>c]</sup>	0.179 <sup>c]</sup>	0.258 <sup>c,d]</sup>
<b>July</b>							
DP	Manure Ash & N	0.823	0.133	0.204 <sup>b</sup>	0.486		
DP	NH <sub>3</sub> loss	0.823	0.133		0.513		
CLB-CB	Manure & Compost Ash & N	0.823	0.133	0.550 <sup>b</sup>	0.140	0.041	0.099 <sup>d</sup>
CLB-CB	NH <sub>3</sub> loss	0.823	0.133		0.225	0.039	0.186 <sup>d</sup>

<sup>a</sup> DP = caged layer deep-pit manure storage, CLB = caged layer manure belt, and CB = compost building.

<sup>b</sup> Remainder term using (feed N - egg N - total emission N)

<sup>c</sup> Values believed to be high. Caged layer fans were being modulated. Compost building fans were not in full operation.

<sup>d</sup> Base on Total NH<sub>3</sub>-N loss - NH<sub>3</sub>-N loss CLB.

Total losses of NH<sub>3</sub>-N, using manure or compost N levels, for the July test showed (table 3) similar values to the March study, with 0.486 kg (1.07 lb) N bird<sup>-1</sup> yr<sup>-1</sup> for DP and 0.140 kg (0.308 lb) N bird<sup>-1</sup> yr<sup>-1</sup> for the CLB-CB. Thus, NH<sub>3</sub> losses for the CLB-CB system were 29% of the deep-pit system in the July study. The NH<sub>3</sub> losses from the laying house in July for the CLB-CB system were estimated at 0.040 kg bird<sup>-1</sup> yr<sup>-1</sup>, compared to 0.034 kg bird<sup>-1</sup> yr<sup>-1</sup> cited by Groot Koerkamp (1994). These results show that the belt/compost system has a major advantage over the deep-pit system in terms of ammonia emissions. For the DP and CLB-CB systems, the calculated NH<sub>3</sub>-N losses in July using airflow rates and ammonia concentrations in the exhaust air were 0.513 and 0.225 kg (1.129 and 0.495 lb) N bird<sup>-1</sup> yr<sup>-1</sup>, respectively. Again, results using airflows and NH<sub>3</sub> concentrations were approximate because airflows were varying during the data collection period. For the conventional deep-pit caged layer system, the exhaust streams measured 7 to 25 ppm NH<sub>3</sub> v/v when all exhaust fans (32 per building) were running, while the belt caged layer system had 1 to 1.5 ppm NH<sub>3</sub> v/v (Keener et al, 2002).

## Discussion

Results using nitrogen and ash levels for determining upper limits for NH<sub>3</sub> emissions for the caged layer facilities studied gave NH<sub>3</sub> emission values similar to those reported in the literature. The N/ash method was straightforward to implement and appears to be reasonably accurate. Values for July were similar to those for March, namely 0.129 and 0.140 kg NH<sub>3</sub>-N bird<sup>-1</sup> yr<sup>-1</sup> for CLB-CB and 0.477 and 0.486 kg NH<sub>3</sub>-N bird<sup>-1</sup> yr<sup>-1</sup> for the DP systems, respectively. Emission values calculated using airflow rates and gas concentrations were 20% to 250% higher and were subject to much greater uncertainty. The problem was that airflows were non-steady state in the March tests. With variable airflow rates, NH<sub>3</sub> levels in the pit increased with low airflow and decreased with high airflow and were dependent on previous airflow rates. This is because NH<sub>3</sub> emission from manure is affected by pit air and manure NH<sub>3</sub> levels, which in turn are affected by prior events. In July, airflow rates were essentially constant with all fans running at maximum output; thus, the resulting emission rates using airflow were much closer to the values based on manure nitrogen. The results clearly showed that the CLB-CB system would have  $\cong$ 28% less emissions than the DP system. In addition, from the standpoint of N conservation, the CLB-CB compost retained over twice as much nitrogen as the DP manure while being a dry product at 82% to 90% dry matter and 5.6% to 6.2% N.

## Conclusions

The method of using ash as a reference value in calculating NH<sub>3</sub> emissions for caged layer poultry was an accurate and straightforward way to determine the upper limits of emissions on a per bird basis. This approach is lower cost, easily implemented and can provide accurate estimates of the upper limits on NH<sub>3</sub> emissions than the current methods of quantifying airflow rates and NH<sub>3</sub> concentrations in exhaust streams.

## Acknowledgements

This paper was adapted from the paper by Keener and Michel (2005) given at the Symposium on the State of Science of Animal Manure and Waste Management, San Antonio, TX. Salaries and research support are

provided by the State and Federal funding appropriated to the Ohio Agricultural Research and Development Center, The Ohio State University. Use of a commercial trade name or company in this paper does not imply endorsement of the products but is included only to assist the reader.

### References

- Battye, R., W. Battye, C. Overcash, and S. Fudge. 1994. Development and selection of ammonia emission factors. Final report prepared for USEPA Contract Number 68-D3-0034. Washington, D.C.: U.S. EPA.
- Groot Koerkamp, P. W. G. 1994. Review on emissions of ammonia from housing systems for laying hens in relation to sources, processes, building design, and manure handling. *J. Agric. Eng. Res.* 59(2): 73-87.
- Heber, A.J., J.Q.Ni, B.L. Haymore, R.K. Duggirala, and K.M. Keener. 2001. Air quality and emission measurement methodology at swine finishing buildings. *Transactions of ASAE* 44(6):1765-1778.
- Keener, H.M., D.L. Elwell, and D. Grande. 2002. NH<sub>3</sub> emissions and N-balances for 1.6 million caged layer facility: manure belt/composting system vs deep pit operation. *Transactions of ASAE.* 45(6):1977-1984.
- Keener, H.M. and F.C. Michel Jr. 2005. Predicting NH<sub>3</sub> emissions from manure N for caged layer facilities. A modified mass balance approach. Symposium on the State of Science of Animal Manure and Waste Management. 1/5-7. Marriott River Center, San Antonio, TX. Published on CD (search at: [http://www.cals.ncsu.edu/waste\\_mgt/natlcenter/sanantonio/proceedings.htm](http://www.cals.ncsu.edu/waste_mgt/natlcenter/sanantonio/proceedings.htm))
- NRC. 2003. Air Emissions from Animal Feeding Operations: Current Knowledge, Future Needs. The National Research Council of the National Academies. The National Academies Press, Washington, D.C.
- Yang, P., J. C. Lorimor, and H. Xin. 2000. Nitrogen losses from laying hen manure in commercial high-rise layer facilities. *Trans. ASAE* 43(6): 1771-1780.



## Ozone Damage to Crops in Southern Africa: An Initial Modeling Study

M. Zunckel<sup>1</sup>, L.D. Emberson<sup>2</sup> and M. Sowden<sup>1</sup>

<sup>1</sup>CSIR, P O Box 17001, Congella 4013, South Africa

<sup>2</sup>Stockholm Environmental Institute, University of York, Heslington, York YO10 5DD

### Abstract

The Cross Border Impact Assessment Project (CAPIA) was designed to develop an understanding of regional surface ozone concentrations and their potential risk to agriculture in southern Africa. Surface ozone concentrations were estimated using the Comprehensive Air Quality Model with extensions (CAMx). The initial assessment of ozone risk to maize was characterised using the Accumulated exposure Over a Threshold of 40 ppb (AOT40). Modelled ozone concentrations exceed 40 ppb over much of southern Africa, suggesting that the potential for ozone damage to maize exists across the region. The AOT40 approach has limitations; the most notable being its inability to account for modifying factors that limit the amount of pollutant taken up by the plant. The aim of this research is to investigate the feasibility of including the stomatal flux algorithms in the CAMx model, and so improve the estimates of ozone uptake in plants and the subsequent risk of ozone damage posed to crops. The initial model results indicate that the areas with elevated ozone concentrations are not the same as those with the highest ozone fluxes, suggesting that application of the more biologically relevant flux-based risk assessment methods would identify different regions within the modelling domain where damage to maize is more likely to occur. In addition, the algorithms in CAMx tend to underestimate both the deposition velocity and ozone flux in comparison to the flux method. Lastly, the maximum modelled total ozone fluxes are above the critical stomatal flux values of  $6 \text{ nmol m}^{-2} \text{ s}^{-1}$  currently defined and applied within Europe to assess risk and economic impacts of ozone to agricultural crops.

### Introduction

In many parts of the world surface ozone is considered to be the most prevalent and damaging air pollutant to which plants are exposed (Emberson *et al*, 2001a). Precursor emissions from multiple source types in the southern African region include those from biomass burning (Scholes *et al*, 1996), large and small industry and mining, transport (Fleming and van der Merwe, 2002) and the combustion of wood and fossil fuels in domestic areas. In addition, natural emissions from biogenic sources have been shown to be significant (Greenberg *et al*, 2003; Harley *et al*, 2003). With high insolation and a dominant anticyclonic circulation that imposes long atmospheric residence times for the mixture of pollutants, an ideal environment exists in which ozone can form. Indeed, monitoring at Maun, a remote rural site in Botswana (Zunckel *et al*, 2004) has indicated that ozone concentrations in this remote area often exceed those typically experienced in urban environments. Despite this, surface ozone is monitored at only a few sites. With the exception of the Global Atmosphere Watch station at Cape Point where surface ozone concentrations have been logged since 1983 (Brunke and Scheel, 1998), the measurement records cover relatively short time periods. This dearth of ozone data implies that the understanding of surface ozone concentrations over the region is limited as is the understanding of potential impacts on vegetation.

Following suggestions by van Tienhoven *et al* (2005) that southern African vegetation may be at risk to damage by ozone, the Cross Border Air Pollution Impact Assessment (CAPIA) project was designed to develop an understanding of regional scale surface ozone concentrations, and to assess the potential risk of air pollution on agriculture. In the absence of comprehensive monitored ozone data, a modelling approach was required to meet the objectives of CAPIA. Using available data on anthropogenic and biogenic emissions and regional scale meteorology, ambient surface ozone concentrations were estimated using the Comprehensive Air Quality Model with Extensions (CAMx) (ENVIRON, 2003). The European approach known as the Accumulated exposure Over a Threshold of 40 ppb (AOT40) (Fuhrer *et al*, 1997) was used to assess the risk to maize in the CAPIA project. van Tienhoven *et al* (2006) identified that the AOT40 was exceeded over large areas of southern Africa and suggested that maize and other agricultural crops were indeed at risk to ozone damage.

The AOT40 is an approach that identifies the potential risk of ozone damage to vegetation based on the ambient concentration to which the plant is exposed (Fuhrer et al. 1997). This approach has some limitations; the most notable being its inability to account for modifying factors that limit the amount of pollutant actually taken up by the plant. These generally occur through modifications to stomatal conductance caused by local environmental conditions such as low humidities and high soil water stresses (Musselman and Massman, 1999). These factors are not considered by the AOT40 approach since damage is only related to the external pollutant concentration rather than the absorbed pollutant dose. The limitations of using only the AOT40 approach for the CAPIA risk assessments were recognised and resulted in the decision to use the recently developed “flux based” risk assessment method

This paper provides an overview of the theory and standard approach used in CAMx to calculate dry deposition of ozone. It also provides a theoretical discussion of the “flux modelling”, emphasising the differences between the two methodologies. An initial comparison between ambient concentrations calculated using the standard CAMx dry deposition for ozone and the flux algorithms are presented.

## Methods

### Dry Deposition Modelling in CAMx

Analogous to an electrical circuit, the movement of aerosols or gases through a plant canopy and onto plant surfaces and the ground surface is typically modelled as a combination of resistances in series and parallel. Each branch of the circuit represents a different path by which material may be deposited. For example, pollutants may transfer to the sites of biological action within the leaves of the plant canopy through the stomatal openings to the mesophyll tissue. They may also deposit on the external surfaces of the plant canopy or move through the canopy and deposit directly on the ground surface. As ozone is a gas, this discussion considers deposition of gases only.

The factor that links the rate of dry deposition of a gas to the ambient concentration is the deposition velocity, where

$$F = -V_d * C \quad (\text{Eq. 1})$$

$C$  is the ambient concentration of the gas,  $V_d$  is the deposition velocity and  $F$  is the deposition rate or flux. The negative notation indicates a downward flux. The ambient concentration is typically measured or modelled, the latter being the case within the CAPIA project. Wesley and Hicks (1977) and later Wesley (1989) developed a resistance model that incorporates the major resistances to deposition which may be described by the following equation:

$$V_d = \frac{1}{R_a + R_b + R_s} \quad (\text{Eq. 2})$$

$R_a$  is the aerodynamic resistance and represents bulk transport between some reference height and the plant canopy. In the case of the CAMx modelling performed within the CAPIA project this height is 10 m above the ground surface. The pollutant transport within this part of the atmosphere results from turbulent diffusion. The magnitude of the  $R_a$  term depends on the intensity of turbulent motion, which in turn, depends on insolation, wind speed, surface roughness and the near-surface lapse temperature rate. As a result,  $R_a$  is a minimum on warm sunny days with strong mixing induced by surface heating and mechanical turbulence and a maximum on cool nights with calm winds and suppressed mixing.

In CAMx (ENVIRON, 2003)  $R_a$  is calculated from:

$$R_a = \frac{1}{ku_*} \left[ \ln \left( \frac{z}{z_0} \right) - \Phi_h \right] \quad (\text{Eq. 3})$$

where

- $u_*$  frictional velocity (m/s), which is a function of the landuse type which is an input requirement in CAMx.
- $k$  von Karman constant.
- $z$  reference height (10m)

$z_0$  roughness length, which is also a function of landuse.  
 $\Phi_h$  stability correction term.

$R_b$  is the quasi-laminar sub-layer resistance that represents molecular diffusion through the thin layer of air that is directly in contact with the surface to which deposition takes place. It is mostly dependant on the molecular diffusivity of each pollutant species, which in turn is dependant on the friction velocity ( $u_*$ ), von Karman's constant ( $k$ ) and the Schmidt number ( $S_c$ ) which is the ratio of air viscosity to molecular diffusivity of the chemical species.

$$R_b = \frac{2S_c^{2/3}}{ku_*} \quad (\text{Eq. 4})$$

The surface resistance,  $R_s$ , is expressed as a combination of serial and parallel resistances that depend on the physical and chemical characteristics of the surface in question. Over vegetated land surfaces  $R_s$  is given by the following equation:

$$R_s = \frac{1}{\frac{1}{r_{st} + r_m} + \frac{1}{r_{uc}} + \frac{1}{r_{dc} + r_{cl}} + \frac{1}{r_{ac} + r_{gs}}} \quad (\text{Eq. 5})$$

The first serial resistance represents the pathway into the stomatal and mesophyll portions of the active plant. The second resistance represents the pathway into the upper canopy and the third is the pathway into the lower canopy. The fourth resistance is the pathway to the ground surface. Some of the resistances are dependant on season and landuse type which are included in the dry deposition model (Wesley, 1989), and so included in CAMx. Other resistances are adjusted in CAMx to account for variation in insolation, moisture stress and surface wetness.

The CAMx modelling domain is typically divided into user defined spatial grids. The underlying surface is gridded accordingly and variations in land use type across the modelling domain are captured in the model by the allocation of the dominant land use category to each grid block. The plant specific resistance algorithms described above are then scaled-up by applying them in each grid block.

### The European Flux Model

In the European flux model, total ozone deposition velocity is also calculated using the 3-resistance formulation (Eq.2), similar to Wesley's (1986) method which is used in CAMx. The resistances include the aerodynamic resistance ( $R_a$ ), the boundary layer resistance ( $R_b$ ) and the surface resistance ( $R_{sur}$ ).  $R_a$  and  $R_b$  are calculated using the same principles described in equations 3 and 4 respectively.  $R_{sur}$  comprises a plant canopy resistance and a resistance to the underlying soil similar to the Wesley (1989) approach. It is given by:

$$R_{sur} = \frac{1}{\frac{LAI}{R_{sto}} + \frac{LAI}{R_{ext}} + \frac{1}{R_{inc} + R_{soil}}} \quad (\text{Eq. 6})$$

where

$R_{inc}$  canopy aerodynamic resistance  
 $R_{soil}$  soil resistance  
 $R_{ext}$  external resistance  
 $R_{sto}$  land cover-specific stomatal resistance which is the resistance to ozone uptake through the stomata  
 $LAI$  leaf area index,

$R_{ext}$  and  $R_{soil}$  are constants.  $R_{inc}$  is calculated with:

$$R_{inc} = \frac{(b * LAI * h)}{u_*} \quad (\text{Eq. 7})$$

where

$b$  an empirical constant taken as  $14 \text{ m}^{-1}$   
 $h$  the vegetation height  
 $u^*$  friction velocity

A schematic of the various resistances and their configuration is presented in Figure 1.

One of the key differences between the CAMx and European deposition models is the approach to calculating stomatal resistance. To incorporate certain aspects of the European deposition model into the CAMx model two modules were developed. Module 1 is a canopy stomatal resistance module and Module 2 is a leaf stomatal flux module. The application of the former can be used to calculate total dry deposition to maize using the stomatal formulations that are unique to the European deposition model. This will allow comparisons of dry deposition to maize that are solely dependant upon the calculation of the stomatal component, considered a key component of total deposition during the growing season. The application of Module 2 would give an indication of the ozone uptake to upper canopy leaves of maize. Comparisons of the spatial pattern of cumulative ozone flux with AOT40 could then be used to assess the consequences of using concentration rather than flux based approaches to identify the risk posed to vegetation from surface ozone.

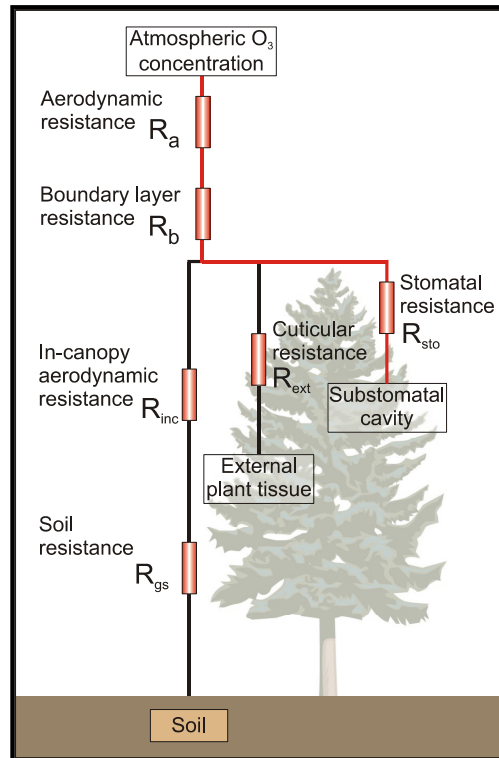


**Figure 1: A schematic of the resistances to dry deposition of a pollutant gas (Emberson et al. 2001b)**

Module 1 was developed to take the place of the existing stomatal resistance (defined by  $r_{st}$  in CAMx as in Eq. 8). The existing  $r_{st}$  is used to estimate surface resistance and is incorporated in the overall resistance scheme according to the parallel resistance approach of Wesley and Hicks (1977) and Wesley (1989). The stomatal resistance ( $r_{st}$ ) is calculated with:

$$r_{st} = \text{diffRACT} * r_j * (1 + (200 / (\text{solflux} + 0.1))^2) * (400 / (t_s * (40 - t_s))) \quad (\text{Eq. 8})$$

where

## Workshop on Agricultural Air Quality

diffraction	ratio of molecular diffusivity of water to species;
$r_j$	baseline minimum stomatal resistance (s/m);
solflux	solar radiation flux ( $W\ m^{-2}$ );
$t_s$	surface temperature ( $^{\circ}C$ ).

In the European flux model Module 1 replaces the calculation of  $r_{st}$  (described above) with  $R_{sto}$  (described below). Module 2 calculates  $g_{sto}$  (stomatal conductance in  $mmol\ O_3\ m^{-2}\ s^{-1}$  on a projected leaf area basis). From the latter, stomatal ozone flux to a representative leaf at the top of the canopy could be calculated.

Parameters that are applied in the Module 1 and 2 for maize are listed in Table 1.

### *Module 1: Canopy Stomatal resistance ( $R_{sto}$ )*

Module 1 calculates canopy stomatal resistance ( $R_{sto}$ ) in units of  $s\ m^{-1}$  according to :-

$$R_{sto} = [(g_{max} * f_{phen} * f_{light} * \max\{f_{min}, (f_{temp} * f_{VPD} * f_{SWP})\}) / 41000]^{-1} \quad (\text{Eq. 9})$$

41000 is the factor to convert from  $mmol\ m^{-2}\ s^{-1}$  to  $m\ s^{-1}$  (Jones, 1992).

$g_{max}$	is the maximum stomatal conductance in units of $mmol\ O_3\ m^{-2}\ s^{-1}$ expressed on a projected leaf area basis
$f_{phen}$	is the relative f determined by leaf age
$f_{min}$	is the minimum daytime stomatal conductance observed under field conditions
$f_{light}$	is the relative mean canopy f determined by irradiance
$f_{temp}$	is the relative f determined by temperature
$f_{VPD}$	is the relative f determined by the leaf-to-air vapour pressure deficit (VPD)
$f_{SWP}$	is the relative f determined by the soil water potential (SWP), (related to soil moisture deficit, SMD)

The relative g factors are expressed on a scale of 0-1 and used to modify  $g_{max}$ . Capitals denote the whole canopy value; small case denotes a single leaf.

The variables required to calculate  $R_{sto}$  in Eq. 10 are either assigned constant values (Table 1) or calculated using the following set of equations:

**Table 1: Parameters applied in the calculation of  $R_{sto}$  and  $g_{sto}$ .**

Parameter	Description	Value	Unit
$R_{ext}$	Resistance of the exterior plant parts to uptake or destruction of ozone	2500	s/m
$R_{soil}$	Resistance to destruction or absorption at the soil surface	200	s/m
$LAI_{max}$	Maximum LAI during the growing season	3.5	$M^2/m^2$
$h$	Maximum plant height	2	M
$g_{max}$	maximum stomatal conductance in units of $mmol\ O_3\ m^{-2}\ s^{-1}$ expressed on a projected leaf area basis	150	$mmol\ O_3\ m^{-2}\ s^{-1}\ (P)$
$f_{phen}$	Relative $g$ determined by leaf age	1	
$f_{min}$	Minimum daytime stomatal conductance observed under field conditions	0.2	
$f_{light}$	relative mean canopy $g$ determined by irradiance	see function	
$\alpha$	for $f_{light}$ function	-0.005	
$f_{temp}$	relative $g$ determined by temperature	see function	
$T_{min}$	for $f_{temp}$ function	0	
$T_{opt}$	for $f_{temp}$ function	25	
$T_{max}$	for $f_{temp}$ function	51	
$f_{VPD}$	relative $g$ determined by the leaf-to-air vapour pressure deficit (VPD)	see function	
$VPD_{max}$	for $f_{VPD}$ function	1	
$VPD_{min}$	for $f_{VPD}$ function	2.5	
$f_{SWP}$	relative $g$ determined by the soil water potential (SWP), (related to soil moisture deficit, SMD)	see functions	

### Irradiance ( $f_{light}$ )

For Module 1, the application of a canopy radiative transfer model is necessary to estimate the influence of irradiance (which changes with canopy depth) on the stomatal conductance ( $g_{sto}$ ) of sunlit and shaded leaf portions of the canopy.

The  $f_{light}$  function requires radiation measured as photosynthetically active radiation (PAR) in  $\mu mol\ m^{-2}\ s^{-1}$ .

$$PAR\ (\mu mol\ m^{-2}\ s^{-1}) = \text{Solar radiation (Wm}^{-2}) / 2 * 4.57 \quad (\text{Eq. 10})$$

Application of the canopy radiative transfer model requires the evaluation of the solar elevation ( $\sin\beta$ ) to relate the “height” of the sun in the sky with the penetration of irradiance into the canopy.  $\sin\beta$  is calculated according to the following equation, with angles in degrees.

$$\text{solar declination } (\delta) = -23.4 * \text{COS}(360*(\text{day of year}+10)/365) \quad (\text{Eq. 11})$$

$$\sin\beta = \sin(\text{latitude}) * \sin(\delta) + \cos(\text{latitude}) * \cos(\delta) * \text{time of day function} \quad (\text{Eq. 12})$$

The canopy radiative transfer model is used to estimate the PAR for both sunlit and shaded canopy portions. This requires that the  $I_{dir}$  and  $I_{diff}$  fractions of the total PAR are calculated. This is achieved using a simplified version of the method developed by Weiss & Norman (1985) to estimate the fraction of PAR that is direct irradiance ( $I_{dir}$ ) using equation 14. The remaining fraction being the diffuse irradiance component ( $I_{diff}$ ):-

$$I_{dir} = -0.000000084 * PAR^2 + 0.00041 * PAR + 0.4075 \quad (\text{Eq. 13})$$

$$I_{diff} = 1 - I_{dir} \quad (\text{Eq. 14})$$

The respective fractions of direct and diffuse irradiance can then be used to estimate the absolute irradiance at the top of the canopy.

$$I_{dir} = I_{f_{dir}} * PAR \quad (Eq. 15)$$

$$I_{diff} = I_{f_{diff}} * PAR \quad (Eq. 16)$$

The necessary input parameters are then available to apply the canopy radiative transfer model so that the irradiance falling on the sunlit and shaded portions of the canopy as a whole can be estimated:-

$$PAR_{shade} = I_{diff} * \exp(-0.5 * LAI^{0.7}) + 0.07 * I_{dir} * (1.1 - 0.1 * LAI) * \exp[-\sin\beta] \quad (Eq. 17)$$

$I_{diff}$  is the flux density of diffuse PAR above the canopy. LAI is the leaf area index

$$PAR_{sun} = I_{dir} * \cos(\theta) / \sin\beta + PAR_{shade} \quad (Eq. 18)$$

$I_{dir}$  is the flux density of direct PAR above the canopy.

$\theta$  is the angle between a leaf and the sun and is assumed to be constant to 60 degrees.

$PAR_{sun}$  and  $PAR_{shade}$  are the flux densities of PAR on sun and shaded leaves. Scaling from the leaf to canopy level is achieved by calculating  $f_{light}$  [equation 20 to 24] for sunlit and shaded fractions proportionally (in terms of LAI) for the whole canopy. Where:

$$f_{lightSun} = [1 - \exp(-\alpha * PAR_{sun})] \quad (Eq. 19)$$

$$f_{lightShade} = [1 - \exp(-\alpha * PAR_{shade})] \quad (Eq. 20)$$

$$LAI_{sun} = [1 - \exp(-0.5 * LAI / \sin\beta)] * 2 \sin\beta \quad (Eq. 21)$$

$$LAI_{shade} = LAI - LAI_{sun} \quad (Eq. 22)$$

$$f_{light} = f_{lightSun} * LAI_{sun} / LAI + f_{lightShade} * LAI_{shade} / LAI \quad (Eq. 23)$$

$f_{lightSun}$  is the  $f_{light}$  value for sunlit leaves

$LAI_{sun}$  is the sunlit leaf area of the canopy.

$LAI_{shade}$  is the shaded area of the canopy

LAI is the leaf area index

$f_{lightShade}$  is the  $f_{light}$  value for shaded leaves

#### Temperature function ( $f_{temp}$ )

The  $f_{temp}$  function estimates the influence of temperature on  $g_{sto}$ . Here it is assumed that temperature is constant with depth throughout the canopy.

$$f_{temp} = \max \{ f_{min}, [(T - T_{min}) / (T_{opt} - T_{min})] * [(T_{max} - T) / (T_{max} - T_{opt})]^{bt} \} \quad (Eq. 24)$$

T is the air temperature in °C,

$T_{min}$  and  $T_{max}$  are the minimum and maximum temperatures at which stomatal closure occurs to  $f_{min}$ ,

$T_{opt}$  is the optimum temperature and

bt is defined as:  $bt = (T_{max} - T_{opt}) / (T_{opt} - T_{min})$

#### Vapour Pressure Deficit function ( $f_{VPD}$ )

The  $f_{VPD}$  function estimates the influence of Vapour Pressure Deficit (VPD) on  $g_{sto}$ . Input data available from CAMx are water vapour mixing ration in ppm ( $w_p$ ) and atmospheric pressure in hPa (p).

Vapour pressure is calculated using the following equations:-

Calculate water vapour in g/kg ( $w_s$ )

$$w_s = (w_p * 1000) / 10^6 \quad (\text{Eq. 25})$$

Calculate vapour pressure in hPa (e)

$$e = \frac{w_s * p}{1000 * 0.622} \quad (\text{Eq. 26})$$

Saturated vapour pressure ( $e_s$ ) in hPa which is a function of temperature is required to convert from vapour pressure to vapour pressure deficit.

$$e_s = 611.21 * \exp\left(\frac{17.502 * T}{240.97 + T}\right) / 100 \quad (\text{Eq. 27})$$

$e_s$ , the saturation vapour pressure is in Pa. T is the air temperature in °C.

The calculation of vapour pressure deficit, VPD, in kPa is then

$$\text{VPD} = \min\{0, (e_s - e) / 100\} \quad (\text{Eq. 28})$$

The resulting VPD value (divided by 1000 to give VPD in kPa) can then be used in the following  $f_{\text{VPD}}$  function:-

$$f_{\text{VPD}} = \min\{1, \max\{f_{\text{min}}, ((1-f_{\text{min}}) * (\text{VPD}_{\text{min}} - \text{VPD}) / (\text{VPD}_{\text{min}} - \text{VPD}_{\text{max}})) + f_{\text{min}}\}\} \quad (\text{Eq. 29})$$

*Soil water status ( $f_{\text{SWP}}$ )*

The CAMx model identifies three levels of soil water potential; these are assigned to the following  $f_{\text{SWP}}$  values, where  $f_{\text{SWP}}$  represents the function deterring the influence of soil water status on  $g_{\text{sto}}$ . Although this is a simplification of the model, only allowing step-changes in  $g_{\text{sto}}$  response to SWP it will provide a spatial indication of the relative importance of the SWP component.

No water stress / irrigated crops  $f_{\text{SWP}} = 1$

Medium water stress  $f_{\text{SWP}} = 0.5$  (Eq. 30)

Extreme water stress  $f_{\text{SWP}} = f_{\text{min}}$

## Module 2: Leaf stomatal conductance ( $g_{\text{sto}}$ )

Module 2 calculates  $g_{\text{sto}}$  (stomatal conductance in  $\text{mmol O}_3 \text{ m}^{-2} \text{ s}^{-1}$  on a projected leaf area basis). From this stomatal ozone flux to a representative leaf at the top of the canopy can be evaluated.

$$g_{\text{sto}} = (g_{\text{max}} * f_{\text{phen}} * f_{\text{light}} * \max\{f_{\text{min}}, (f_{\text{temp}} * f_{\text{VPD}} * f_{\text{SWP}})\}) \quad (\text{Eq. 31})$$

With the exception of  $g_{\text{sto}}$ , the only other variation between Module 1 and Module 2 is in the calculation of irradiance,  $f_{\text{light}}$ . For Module 1 the application of a canopy radiative transfer model is necessary to estimate the influence of irradiance (which changes with canopy depth) on the stomatal conductance of sunlit and shaded leaf portions of the canopy. For module 2, stomatal conductance is estimated only for a leaf in the upper canopy and hence can be calculated simply as a function of the irradiance reaching the top of the canopy as follows:

$$f_{\text{light}} = 1 - \exp(-\alpha * \text{PAR}) \quad (\text{Eq. 32})$$

PAR is the photosynthetically active radiation and  $\alpha$  is constant for  $f_{\text{light}}$ .

The calculation of top leaf stomatal ozone flux ( $\text{fluxO}_3$ ) can then be made using Eq. 33.

$$\text{fluxO}_3 = g_{\text{sto}} * \text{O}_3 \quad (\text{Eq. 33})$$

## Results and Discussion

As an initial method of comparing the CAMx and flux methodologies, a single 50 x 50 km model grid cell over Zimbabwe was selected to investigate model outputs from a 5-day period covering the 10 to 14 January 2001. The results in Fig 3 (top) show clearly the diurnal variation in ozone concentration over Mashonaland, with concentrations reaching more than 90 ppb in the middle of the day. As may be

expected, the deposition velocities ( $V_d$ ) calculated with both the CAMx and the European methodologies (Fig 3, middle) also show strong diurnal variations. However, the  $V_d$  values estimated using the European method are consistently higher than those calculated using the CAMx routine during the daytime periods.

Due to the relationship between the ambient concentration and  $V_d$ , the resultant ozone flux is low at night and reaches maximum values during the daytime period. The European flux model values are consistently greater than those estimated using CAMx. For CAMx, ozone fluxes range from 0 to about  $6 \text{ nmol O}_3 \text{ m}^{-2} \text{ s}^{-1}$ , compared with the European method values, which range from near zero values at night to average daytime maxima of more than  $10 \text{ nmol O}_3 \text{ m}^{-2} \text{ s}^{-1}$ , reaching more than  $15 \text{ nmol O}_3 \text{ m}^{-2} \text{ s}^{-1}$  on 13 January 2001. The higher ozone fluxes estimated using the European model most likely reflect the higher maximum stomatal conductance value assigned to maize in the European model.

It is also interesting to note that the two days with the highest ozone concentrations (10 (0 to 24 hours) and 11 January (24 -48 hours)) are not always those with the highest calculated ozone fluxes. This apparent incongruity would possibly be even more striking if stomatal fluxes were compared with ozone concentrations and highlights the need to use flux rather than concentration based approaches for ozone risk assessments.

The comparison is expanded to a portion of the maize producing area of Mashonaland West to Mashonaland East and Mashonaland Central in Zimbabwe. Here a 550 km by 550 km 'window' is extracted from the southern Africa modelling domain. In Fig 4 each panel represents an area of approximately 300 000  $\text{km}^2$ , running from grid cell 33 to 44 in an east to west direction and from 34 to 44 in a south to north direction. A single modelled value represents each cell. Unlike the diurnal depiction in Fig. 3, the results shown in Fig. 4 are a snap-shot over the defined domain showing results for a single hour, namely 16:00 on 10 January 2001.

For this hour the modelled concentrations of ozone range between 20 and 100 ppb over the model window (Fig. 3, left). Concentrations exceed the threshold value of 40 ppb suggesting that damage to vegetation may be expected over an extensive area covering almost the entire southern half of the window.

One might expect high ozone fluxes to coincide with areas of high ozone concentrations, given the relationship in Eq. 1. Generally speaking this assumption is valid for the CAMx deposition (Fig. 3, centre) with the highest fluxes occurring over the southern parts of the window, ranging from low values and reaching  $6 \text{ nmol O}_3 \text{ m}^{-2} \text{ s}^{-1}$ . It is not a perfect match however, and the area of maximum fluxes occur to the south of the maximum ambient concentrations. The amount of damage predicted by ozone flux models depends on the toxicity of the absorbed dose. The toxicity levels of absorbed ozone to maize growing in southern Africa is not yet known, but European work for wheat and potato has shown that damage could occur at fluxes above  $6 \text{ nmol m}^{-2} \text{ s}^{-1}$ .

As seen in Fig. 3 for the modelling period in cell 38:38, the ozone flux estimated with the European method is consistently higher than that estimated with the CAMx methodology (Fig. 4 centre and right) though there is agreement in the general area where the ozone flux is highest. However, the European model also identifies areas of high ozone fluxes in the northeastern parts of the window (Fig. 4, right).

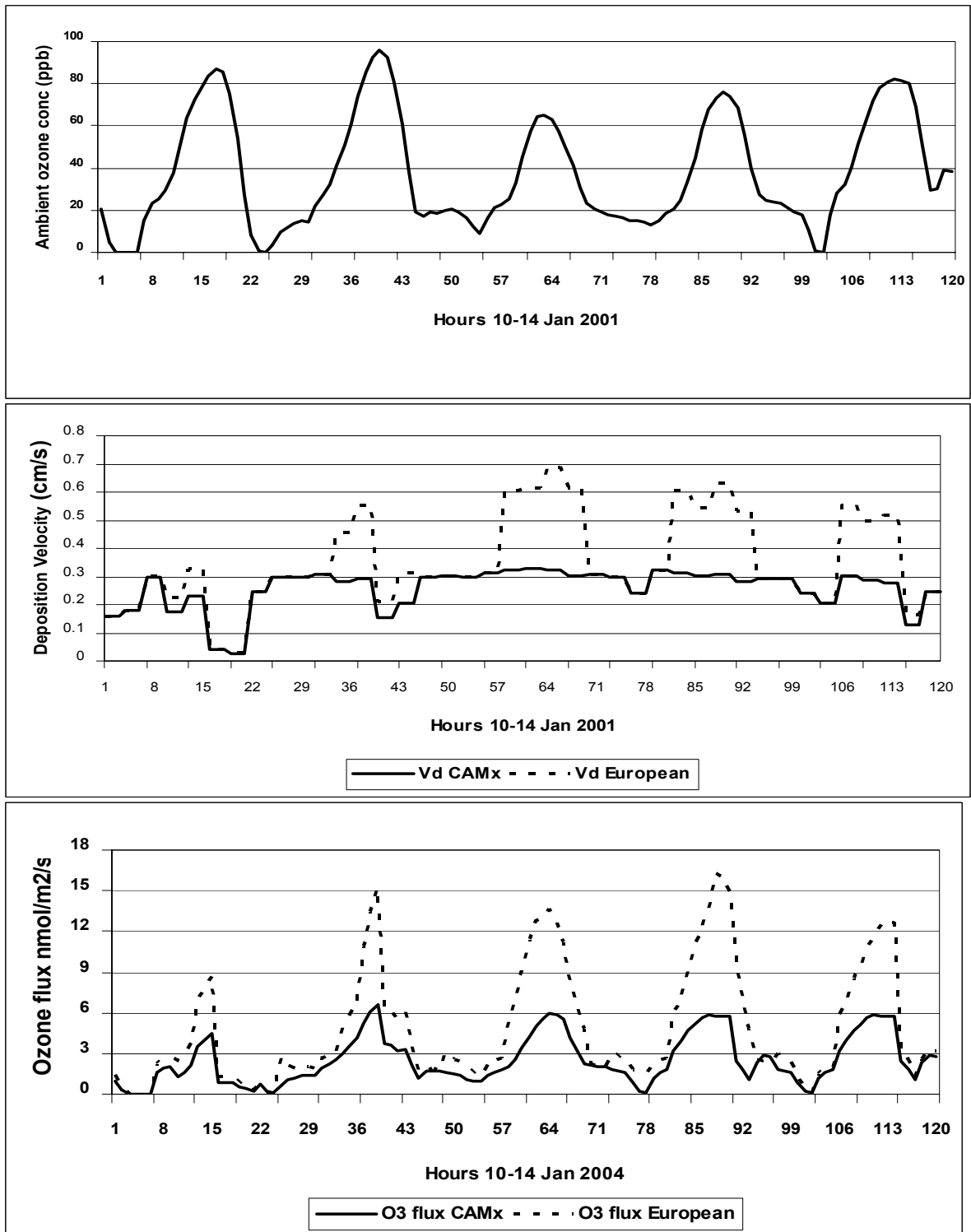
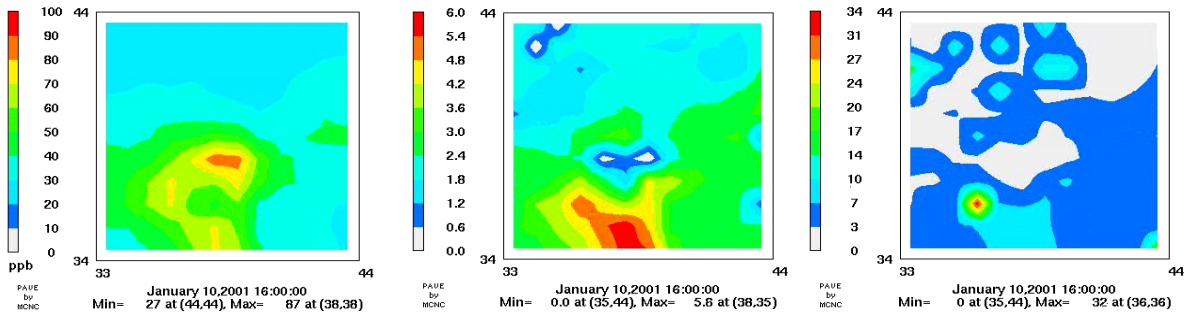
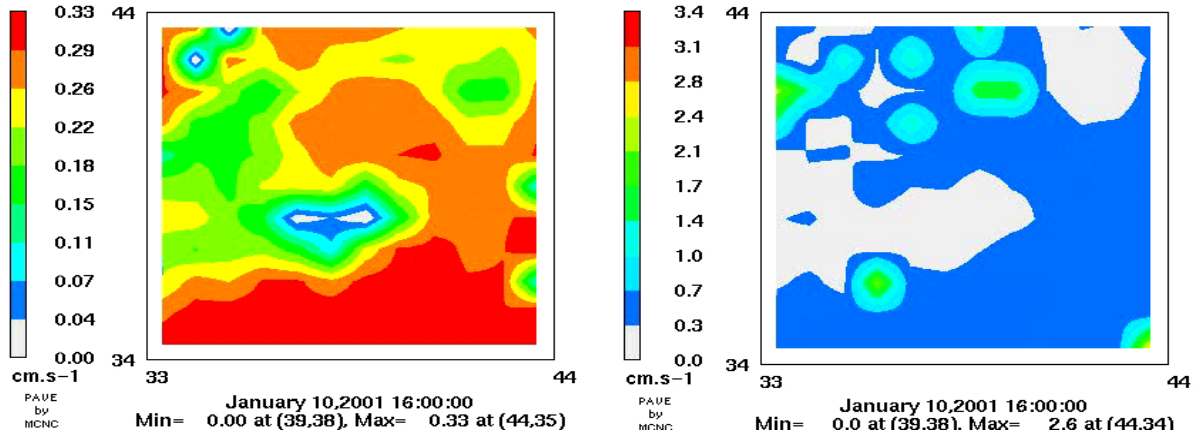


Figure 3: Model results for cell (38:38) in Zimbabwe for 120 hour modelling period 10 to 14 January 2001 with ozone concentration in ppb (top), and the corresponding deposition velocities (centre), and total ozone fluxes (bottom) the latter two components calculated with both the CAMx and European methodologies.



**Figure 4: Modelled ambient ozone concentrations in ppb (left). Modelled CAMx total ozone flux (centre) and modelled flux using the European stomatal flux algorithms over Mashonaland, Zimbabwe at 16:00 on 10 January 2001. Values given in  $\text{nmol O}_3 \text{ m}^{-2} \text{ s}^{-1}$ .**



**Figure 5: Modelled ozone deposition velocity in  $\text{cm s}^{-1}$  over Mashonaland, Zimbabwe at 16:00 on 10 January 2001, estimated with the CAMx (left) and the European flux algorithm (right).**

An interesting comparison is made when evaluating the modelled CAMx ozone fluxes (Fig. 4 centre) and the European ozone fluxes (Fig. 4 right). Again the maximum flux occurs in the south of the window where rates range between 3 and 6  $\text{nmol O}_3 \text{ m}^{-2} \text{ s}^{-1}$  for the CAMx routine. These are generally higher for the European method with ozone fluxes in the south ranging from 3 to more than 30  $\text{nmol O}_3 \text{ m}^{-2} \text{ s}^{-1}$  in one particular area. This is most likely due to the European model being parameterised specifically for maize rather than a more generalised “agricultural” land-cover type. Also interesting is the area of relatively higher ozone fluxes in the northwestern parts of the window predicted using the European method that coincides with relatively low ambient ozone concentrations. This suggests that the incorporation of additional environmental parameters using the European method is able to identify instances when lower ozone concentrations are capable of producing higher ozone fluxes due to the low resistance to ozone uptake and deposition. The European flux estimates reach 14  $\text{nmol O}_3 \text{ m}^{-2} \text{ s}^{-1}$ .

Examination of the deposition velocities ( $V_d$ ) (Fig. 5) adds some additional insights. Again,  $V_d$  calculated with the CAMx algorithms is consistently lower than the European method at 16:00 on 10 January, also seen in Fig. 3. Both approaches return  $V_d$  values in the region of 0.3  $\text{cm s}^{-1}$  over the largest part of the window, but the maximums returned with the European method are much higher than that with CAMx. The highest CAMx values occur in the southwestern part of the window, in the region of 0.35  $\text{cm s}^{-1}$ , decreasing almost consistently towards the northeast. The European flux model shows a contrasting picture

with patches of higher  $V_d$  ranging between 0.3 and 1.7  $\text{cm s}^{-1}$ , with high deposition velocities in the south and in the north east, coinciding with the observed maximums of ozone flux (Fig. 4, right). It is useful to make preliminary comparisons of the model output values with deposition velocities for maize measured under field conditions to give some indication of how well the different models are performing. Deposition velocities for maize growing in The Netherlands were measured by van Pul & Jacobs (1994). These measurement data found  $V_d$  values in the range of 0.2 to 1.6  $\text{cm s}^{-1}$  which would indicate that the predictions of deposition velocity made using the European stomatal flux algorithms are closer to realistic values for this species. However, additional work will be necessary to fully understand the model outputs in relation to observed measurements under location specific climatic conditions.

## Conclusions

It is commonly recognised that using concentration based approaches, such as the AOT40, to assess potential damage to agricultural crops has some limitations. The most notable of these are due to the modifying factors that limit the amount of pollutant actually taken up by the plant and hence uncouple the relationship between concentration and damage. These generally occur through modifications to stomatal conductance caused by local environmental conditions such as low humidities and high soil water stresses. These factors are not considered by the AOT40 approach since damage is only related to the external pollutant concentration rather than the absorbed pollutant dose.

As such, a “flux based” risk assessment method (currently being developed as part of an ozone deposition model for use in Europe) has been applied in this work to assess the possibility of using an additional, more biologically relevant risk assessment method within the CAPIA project. The aim of the work was to initiate the application of certain components of the European deposition module in the standard CAMx model, in particular to investigate the feasibility of including the stomatal flux algorithms, and so improve the estimates of ozone uptake in plants and the risk posed to crops.

The modification of the CAMx model has been successfully completed and initial results, using a single day’s model output over Zimbabwe, illustrate the perceived risk across the region using both concentration and flux based approaches. Analyses of these data highlight the spatial differences between ambient concentrations as calculated for CAPIA, and ozone fluxes calculated by both the CAMx and European deposition models. The main conclusions of this research are:

- Modelled ambient ozone concentrations exceed the 40 ppb threshold over much of southern Africa. This would suggest that application of the concentration based (AOT40) risk assessment method would indicate the potential for ozone damage to maize in the region.
- The areas where ozone concentrations are elevated are not the same as those with the highest ozone fluxes. This suggests that application of the more biologically relevant flux-based risk assessment methods would identify different regions within the modelling domain as being those where most damage to maize is likely to occur.
- The CAMx model tends to underestimate both the deposition velocity and actual ozone flux in comparison to the flux method. This is most likely due to the flux method modelling for a specific species (i.e. maize) rather than a more generic land-cover type (i.e. agricultural crops).
- The maximum total ozone fluxes are above the critical stomatal flux values of 6  $\text{nmol m}^{-2} \text{s}^{-1}$  currently defined and applied within Europe to assess risk and economic impacts of ozone to agricultural crops.

This preliminary work has shown that both the concentration and flux based approaches indicate that ground level ozone concentrations could result in damage to maize across southern Africa. However, the areas of maize growing identified as being at most risk from ozone varies spatially dependant upon which of the two approaches are used. This is due to the flux-based method reducing the uncertainty of the risk assessment by incorporating modifying factors and relating potential damage to absorbed dose rather than concentration. The initial work has also shown there to be differences between the current approaches to estimating deposition in CAMx compared to the species-specific modelling conducted using the European approach. It is important that the initial work is expanded in order to develop improved understandings of ozone deposition and uptake by agricultural crops.

## References

- Emberson L. D., Ashmore M. R., Murray F., Kuylenstierna J. C. I., Percy K. E., Izuta T., Zheng H., Sheu B. H., Liu C. P., Agrawal M., Wahid A., Abdel-Latif N. M., van Tienhoven M., de Bauer L. I. and Domingos, 2001a. Impacts of air pollutants on vegetation in developing countries, *Water, Air and Soil Pollution*, 130, 107-118.
- Emberson L.D., Ashmore M.R., Simpson D., Tuovinen J.-P., and Cambridge H.M., 2001b Modelling and mapping ozone deposition in Europe. *Water, Air and Soil Pollution*, 130, 577-582.
- ENVIRON, 2003. User's guide to the Comprehensive Air Quality Model with Extensions (CAMx), ENVIRON International Corporation, 101 Rowland Way, Novato, CA 94945.
- Fleming G. and van der Merwe M., 2002. Spatial disaggregation of greenhouse gas emissions inventory data for Africa south of the equator, <http://gis.esri.com/library>
- Fuhrer, J., Skärby, L., and Ashmore, M.R., 1997, Critical levels for ozone effects on vegetation in Europe. *Environmental Pollution*, 97 (1-2), 91-106.
- Greenberg J.P, Guenther A., Harley P., Otter L., Veenendaal E. M., Hewitt C. N., James A. E. and Owen S. M., 2003. Eddy flux and leaf-level measurement of biogenic VOC emissions from mopane woodland of Botswana, *Journal of Geophysical Research*, 108(D13), 8 466, doi:10.1029/2002JD002317,2003.
- Harley P., Otter L., Guenther A. and Greenberg J., 2003. Micrometeorological and leaf-level measurements of isoprene emissions from a southern African savanna, *Journal of Geophysical Research*, 108(D13), 8 468, doi:10.1029/2002JD002592,2003.
- Scholes R. J., Kendall J. and Justice C. O., 1996. Emissions of trace gases and aerosol particles due to vegetation burning in southern Africa, *Journal of Geophysical Research*, 101, D19, 23 677-23 682.
- van Pul W.A.J. and Jacobs A.F.G. (1994) The conductance of a maize crop and the underlying soil to ozone under various environmental conditions, *Boundary-Layer Meteorology*, 69, 83-99.
- Wesley M. L. and Hicks B.B., 1977, Some Factors that affect the deposition rates of sulphur dioxide and similar gases on vegetation, *Journal of the Air Pollution Control Association*, 27(11), 1110-1116.
- Wesley M. L., 1989. Parameterization of surface resistance to gaseous dry deposition in regional-scale numerical models, *Atmospheric Environment*, 23, 1293-1304.
- van Tienhoven A. M., Otter L., Lenkopane M., Venjonoka, K and Zunckel M., 2005. Assessment of ozone impacts on vegetation in southern Africa and directions for future research, *South African Journal of Science*, 101, 143-148.
- van Tienhoven A. M., Zunckel M., Emberson L., Koosailee, A. and Otter L., 2005. Preliminary assessment of ozone impacts to maize (*Zea Mays*) in southern Africa, *Environmental Pollution*, 140(2006), 220-230.
- Zunckel M., Venjonoka K., Pienaar J. J., Brunke E-G., Pretorius O., Koosaliee A., Raghunandan A. and van Tienhoven M. A., 2004. Surface ozone over southern Africa: Synthesis of monitoring results during the Cross Border Impact Assessment project, *Atmospheric Environment*, 38(2004), 6139-6147.